REACTION MECHANISMS AT HIGH ENERGY

V Barger

Department of Physics, University of Wisconsin, USA

CONTENTS

Theoretical activity in hadron physics has closely followed experimental developments. For this reason the organization of this talk closely parallels recent experimental results, with emphasis on interpretations of interesting new data from IHEP, NAL and ISR. The contents are arranged as follows:

I. INTRODUCTION

Until recently, in the energy range over which reaction mechanisms could be studied, contributions from non-asymptotic terms were a significant complicating factor. In elastic scattering, the Pomeron exchange could not be separated from vector and tensor exchanges. In inelastic reactions,

direct channel resonances or low lying exchanges could mask the true nature of the leading exchanges over the few GeV region. Consequently unambiguous tests of basic theoretical ideas and phenomenological models were difficult to come by. Fortunately this situation has changed and the impact of the new data is just now beginning to be felt. Investigations of the higher energy measurements have produced some very encouraging first results. For example the energy dependence of pp elastic scattering through NAL and ISR energy ranges is accounted for by geometrical scaling, which is a natural property of optical models with an energy dependent radius. Relations among total cross sections and inelastic differential cross sections based on SU(3) and universality for the couplings of the exchanges begin to work remarkably well above 6 GeV for both helicity non-flip and flip amplitudes. The large angle scattering data on a variety of reactions are in striking accord with a simple quark constituent rule. These developments among others have contributed to a resurge in optimism in the field. From a patchwork of understanding in various frameworks a unified understanding of reaction mechanisms will hopefully emerge. The promise that the physics of reaction mechanisms would become more transparent at high energies was the basic motivation for workers in this area and recent data provide indications that this promise will materialize.

II. BOUNDS FROM FIELD THEORY

A. Froissart Bound

The suggestion of a possible $\ell n^2\, s$ growth of the ISR total cross section measurements[1†] spurred theoretical interest in models which saturate the energy dependence of the Froissart bound

$$\sigma_t \to \ell n^2\, s$$

The slope of the forward elastic peak, $B_o = d/dt\ \ell n(d\sigma/dt)_{t=0}$, must have a similar asymptotic growth

$$B_o \to \ell n^2\, s$$

In field theory[2,3] and Glauber-type models[4] with this asymptotic behaviour, the elastic, diffractive, and total cross section ratios approach the asymptotic limits

$$\frac{\sigma_{el} + \sigma_{diff}}{\sigma_t} = \frac{1}{2} \qquad \frac{\sigma_{el}}{\sigma_t} \to \text{constant} < \frac{1}{2}$$

when both shadowing effects and fragmentation are included. Here the diffraction cross-section refers to fragmentation with no quantum number exchange. For asymptotic scattering from a nucleus A, the total cross-section on the nucleus is the same as the total cross-section on the nucleon

$$\sigma_t(pA) = \sigma_t(pp)$$

if the nucleon is a black absorbing disc[5]. Total cross-section and elastic slope data[6-9] at the highest available accelerator energies indicate that we are still far from an asymptotic regime if the maximal allowed growth with energy is in fact realized in nature.

B. MacDowell-Martin Bound

The MacDowell-Martin bound on the forward elastic slope parameter

$$B_o \geq \frac{1}{18\pi}\frac{\sigma_t^2}{\sigma_{el}} - \frac{2}{9k^2}$$

has received considerable attention in the past. The $1/k^2$ term is negligible above a few GeV. The

---

† The data can be described by $\sigma_t = (38.4 + 0.5\ \ell n^2\,(\frac{s}{137}))$mb. The size of this empirical $\ell n^2\, s$ term is two orders of magnitude smaller than the Froissart bound:

$$\sigma_t \leq \frac{\pi}{\mu^2}\ell n^2\, s, \quad \frac{\pi}{\mu^2} \simeq 60 \text{ mb}.$$

pp slope data are only about 15% above the lower bound at high energies (Figure 1). Unfortunately, the fact that the data are close to the bound provides no useful information about the impact parameter profile of the elastic amplitude[10,11]. For example with either a Gaussian ($\sigma_{el}/\sigma_t \leq \frac{1}{4}$) or black disc ($\sigma_{el}/\sigma_t \leq \frac{1}{2}$) elastic amplitude profile the slope is related to the cross-sections by the same formula: $B_o = \frac{1}{16\pi}\frac{\sigma_t^2}{\sigma_{el}}$

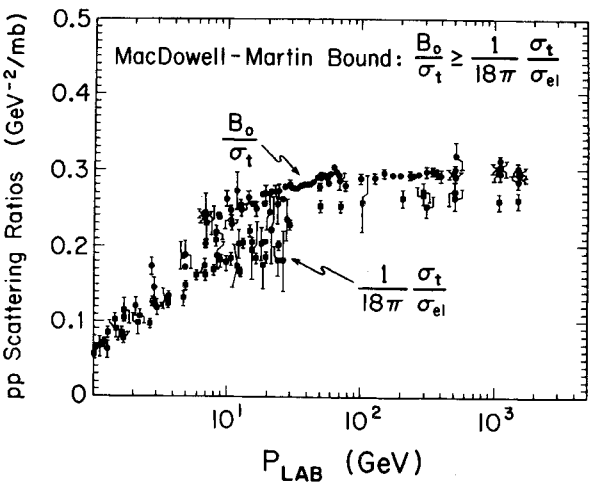

Figure 1: Comparison of pp elastic slope and cross section ratios with the MacDowell-Martin Bound.

III. REAL PARTS OF SCATTERING AMPLITUDES: ANALYTIC DERIVATIVE RELATIONS

Dispersion relations give the real part of a scattering amplitude in terms of an integral over the imaginary part. Evaluation of these non-local relations is a formidable task. Recently Bronzan, Kane and Sukhatme drew attention to the existence of a quasi-local analytic derivative relation[11-13] between real and imaginary parts which is valid at high energies if threshold and resonance effects are unimportant. This derivative relationship provides a simple approximation to conventional dispersion relations for real part calculations†. For elastic amplitudes F normalized as $d\sigma/dt = |F|^2/16\pi$, $\sigma_t = \text{Im } F(s,t=0)$, the derivative relationships are

$$\text{Re } F^+ = \{\tan (\tfrac{\pi}{2}\frac{d}{d\ \ell n\ s})\}\ \text{Im } F^+$$

$$\text{Re } F^- = -\{\cot (\tfrac{\pi}{2}\frac{d}{d\ \ell n\ s})\}\ \text{Im } F^-$$

where, e.g.,

$$F^{\pm} = F(\bar{p}p) \pm F(pp)$$

For forward scattering, data on total cross-section differences are well parameterized by a power law dependence on s,

$$\text{Im } F^- = \beta\ s^{-n},$$

and the derivative relation for the amplitude differences reduces to a standard Regge pole form. For the total cross section sums, the data in successive ranges in s can be well represented by a quadratic in $\ell n\ s$. In this approximation the derivative formula simplifies to

$$\text{Re } F^+ = \frac{\pi}{2}\frac{d}{d\ \ell n\ s}\ \text{Im } F^+$$

Comparisons of derivative calculations of real parts at t = 0 with experiment are shown in Figures 2††. The change in sign of Re F(pp) at 250 GeV is associated with the broad minimum in $\sigma_t(pp)$.

---

† Höhler has questioned the quantitative accuracy of the derivative formula approximation in the πN case. (Ref. 14).

††As in conventional dispersion relations, a subtraction term c/s might contribute to Re F^+ (Ref. 11). Such terms are not considered in the results of Fig. 2.

The derivative relationship can be used at ISR energies to estimate the real part of the scattering amplitude as a function of t[13]. Using the imaginary amplitude from a geometric-scaling description of $d\sigma/dt$ (pp) discussed in Section IV, the real amplitude in Figure 3 is obtained from differentiation with respect to $\ln s$. Re F(pp) changes sign at $t = -0.2$. Re F(pp) is negligible in comparison to Im F(pp) except in the vicinity of the minimum of $d\sigma/dt$ at $t = -1.4$.

IV. PROTON-PROTON SCATTERING

A. Experimental Features

The pp elastic channel provides the most favourable circumstance for the study of the asymptotic diffraction mechanism. The s-channel quantum numbers of pp are exotic, so the imaginary amplitude due to non-diffractive f_o, ω, ρ, A_2 exchanges are expected to be suppressed. Estimates of the energy dependences of the non-diffractive contributions[15] indicate that these exchange contributions are rather small at ISR energies. A common additional approximation in phenomenological descriptions of ISR $d\sigma/dt$ data is the neglect of the real part and spin dependence[16] of the amplitude.

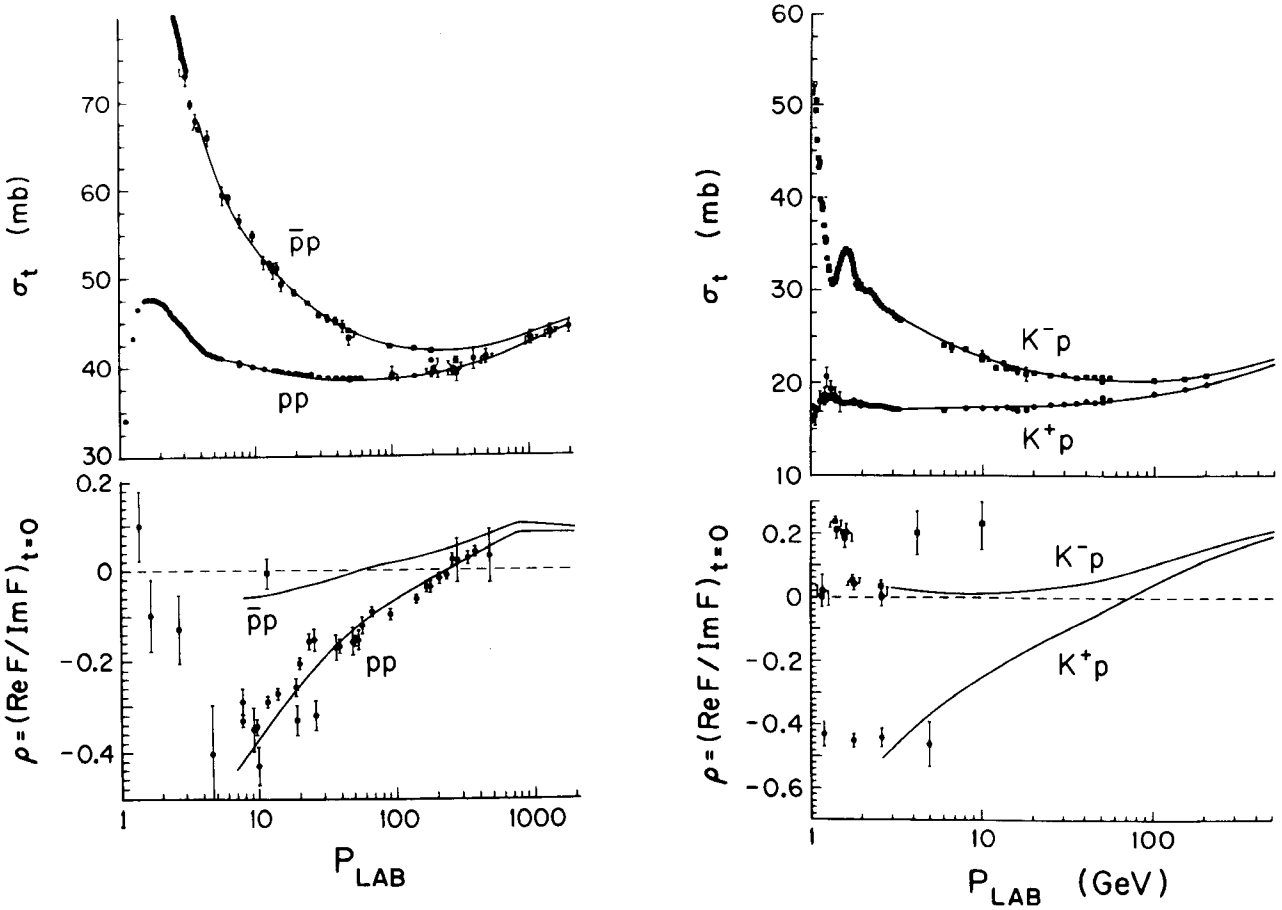

Figure 2: Calculations of forward real parts from derivatives of total sections (cf Ref. 13). (a) $\bar{p}p$, pp (b) K^-p, K^+p

The qualitative experimental properties of pp scattering data over the ISR range ($500 \lesssim s \lesssim 3000$ GeV^2) can be summarized as follows:

(i) Rising Cross-sections

σ_t, σ_{el}, σ_{in} all rise by about 10%[1]. The trends are consistent with $\sigma = \sigma_0 + \sigma_1 \ln s$. (Figure 4). As expected from a rising σ_t, Re $F_{el}(s,t = 0)$ becomes positive above $s = 500$.

(ii) Shrinking Forward Peak

The slope parameter $B_0 \equiv \frac{d\sigma}{dt} (\ln \frac{d\sigma}{dt})_{t=0}$ rises by about 10%[7-9], consistent with $B_0 = b_0 + b_1 \ln s$.

(iii) Constant Cross-Section and Slope Ratios

$$\frac{\sigma_{el}}{\sigma_t} \simeq 0.175 \qquad \frac{B_o}{\sigma_t} \simeq 0.296 \text{ GeV}^{-2}/\text{mb}$$

independent of s. (Figure 5).

(iv) Diffraction Minima in $d\sigma/dt$ at $t = -1.5$

A break in slope of $d\sigma/dt$ for $t \simeq -1.2$ at CERN energies develops into a dip of $d\sigma/dt \simeq -1.4$ at ISR energies[17].

(v) Curvature of $\ln d\sigma/dt$ at Small t

$\ln d\sigma/dt$ has concave curvature for $t \simeq -0.1$. The small t data[6] cannot be parameterized simply as $d\sigma/dt = A\, e^{Bt}$.

These general qualitative features of the data can be described in terms of the combination of phenomenological models, which are discussed next.

B. Phenomenological Framework

Models can be conveniently discussed in terms of the S-matrix element as a function of impact parameter b. In the high energy approximation

$$S(b,s) = e^{-2\delta_I(b,s)}$$

where $\delta_I(b,s)$ is the imaginary part of the phase shift with angular momentum $J = kb$.

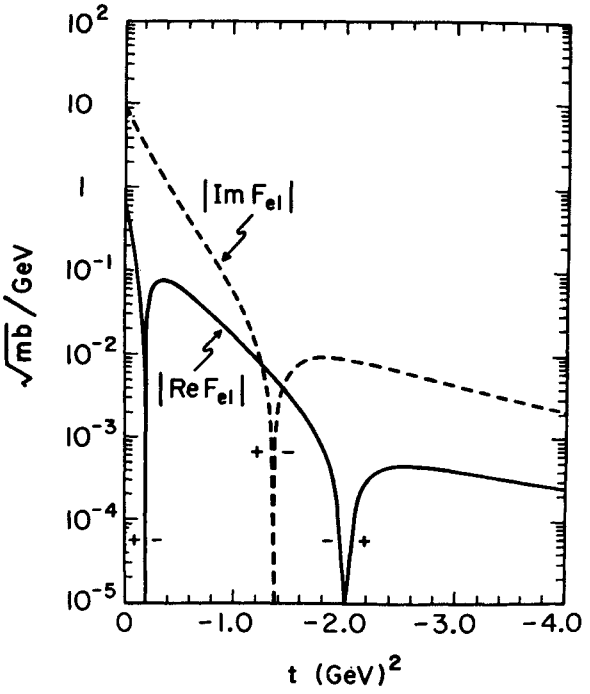

Figure 3: Real part of the pp elastic amplitude at ISR energies as estimated by the analytic derivative method of Ref. 13.

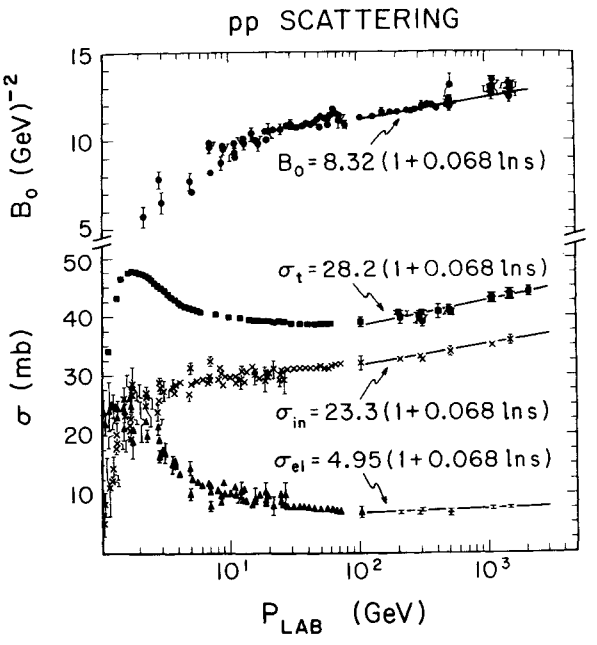

Figure 4: Compilation of pp cross sections and elastic slope parameter (for $|t| \lesssim 0.15$).

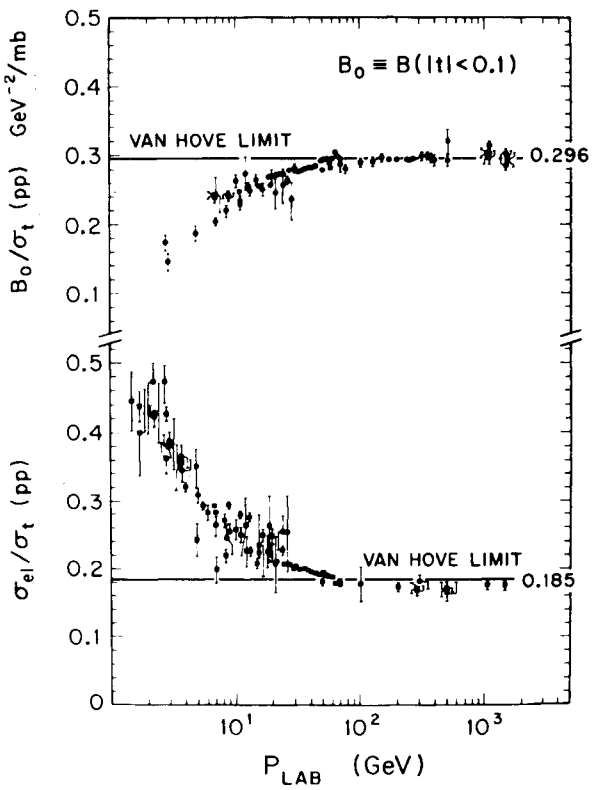

Figure 5: Ratios of pp cross-sections and elastic slope. The Van Hove limits correspond to a Gaussian overlap function of maximum strength allowed by unitarity.

1. Geometrical Scaling

According to the geometrical scaling hypothesis, the energy dependence of the elastic amplitude is entirely contained in an effective radius R(s) and S(b) scales in impact parameter as

$$S(b,s) = \tilde{S}(b/R(s))$$

This scaling behaviour was proposed by Buras and Dias de Deus[18]. Simple optical models, such as a grey disk or a Gaussian in b with constant opacity, have this property.

From geometrical scaling it follows immediately that

$$\sigma_{el} \propto R^2$$

$$\sigma_t \propto R^2$$

$$\sigma_{in} \propto R^2$$

$$B_o \propto R^2$$

$$\frac{d\sigma}{dt} = R^4 \left|\tilde{F}_{el}\left(R\sqrt{-t}\right)\right|^2$$

If the proton radius R(s) grows with s, then geometrical scaling accounts for the growth of σ_t, constant cross-section and slope ratios (σ_{el}/σ_t, B/σ_t), and the shrinkage of the forward elastic peak. The combined ISR data on σ_t, σ_{el}, and B_o are compatible with a $\ell n\, s$ growth of R^2[†].

$$R^2 = R_o^2 + R_1^2 \ell n\, s$$

with $R_o = 0.84$ F

$R_1 = 0.22$ F

The expectation of geometrical scaling that $\frac{1}{\sigma_t^2}\frac{d\sigma}{dt}$ versus $\sigma_t|t|$ should be independent of energy is compatible with the ISR data. (Figure 6a).

The location of the diffraction minimum t_D is predicted by geometrical scaling to move in towards smaller t as s-increases ($|t_D| = c/\sigma_t$). New data from the CERN-Hamburg-Orsay-Vienna collaboration[17] exhibit this inward motion (Figure 6b).

The ratio of $d\sigma/dt$ at the secondary maximum ($t \simeq -2$) to $d\sigma/dt$ at $t = 0$ is predicted to be constant. Consequently if geometrical scaling holds at large t, the rise of the secondary maximum should be proportional to the rise of σ_t^2. The ISR data are consistent with this prediction. (Figure 6b)

The NAL $d\sigma/dt$ (pp) data at 100 and 200 GeV do not establish whether there exists a break in slope at $t \simeq -0.15$ at these energies[20]. However the shape of the NAL data is completely compatible with the

---

[†] Phillips has observed that a Regge dipole ansatz for the Pomeron could satisfy exact geometrical scaling and yield a $\ell n\, s$ growth of R^2. (Ref. 19).

geometrically scaled shape of the ISR data when examined over an identical t-range. (Figure 7)

To discuss the magnitude of σ_{el}/σ_t, the curvature of ℓn dσ/dt at small t, and the existence of the dip at large t, more detailed information about S(b) is needed.

2. Inelastic Overlap Function Model

Since the elastic amplitude at high energy is generated as the shadow of many inelastic channels, Van Hove suggested in 1963[21] that a parameterization of the inelastic overlap function

$$O(b,s) = 1 - |S(b,s)|^2$$

was more basic. Given a model for the inelastic processes, a prediction for elastic scattering follows directly from the unitarity relation (Figure 8)

$$\text{Im } F_{el}(b,s) = |F_{el}(b,s)|^2 + \frac{1}{4} O(b,s)$$

when the real part of F_{el} is neglected. An approximately Gaussian phenomenological behaviour for O(b,s) of maximal strength allowed by unitarity was proposed as first approximation[21].

$$O(b,s) = e^{-b^2/R^2}.$$

For this overlap function the following "Van Hove limits" for cross-section and slope ratios are obtained:

$$\frac{\sigma_{el}}{\sigma_t} = 0.185 \quad \text{(experiment} \simeq 0.175)$$

$$\frac{B_0}{\sigma_t} = 0.296 \quad \text{(experiment} \simeq 0.296)$$

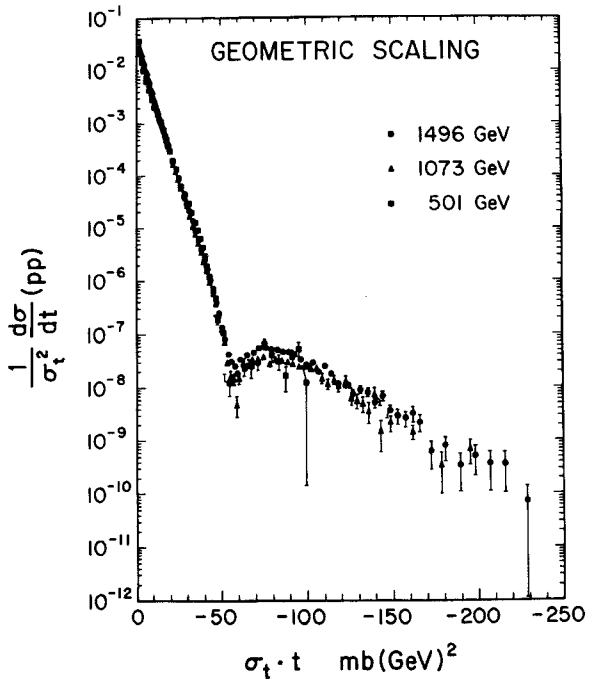

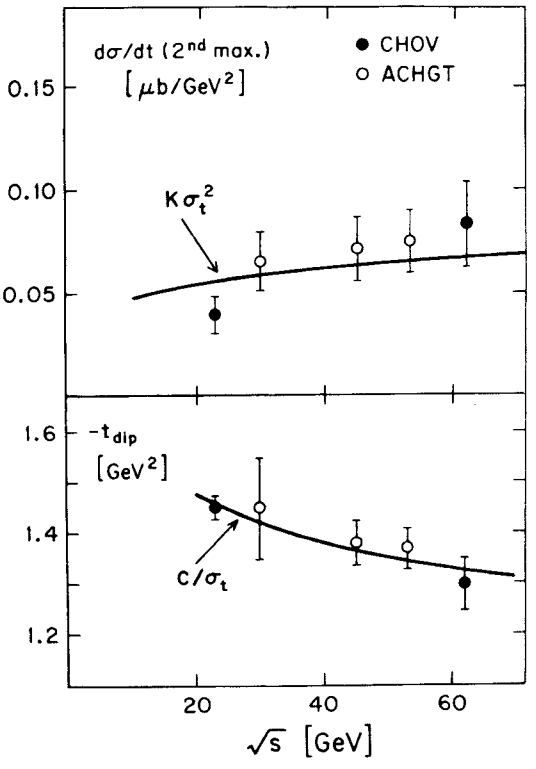

Figure 6: Geometrical scaling of pp elastic scattering data.[17] (a) $(d\sigma/dt)/\sigma_t^2$ versus $\sigma_t|t|$ is predicted to have a universal shape dependent of energy. (b) The dip location is predicted to be proportional to $1/\sigma_t$ and the secondary maximum is predicted to rise like σ_t^2.

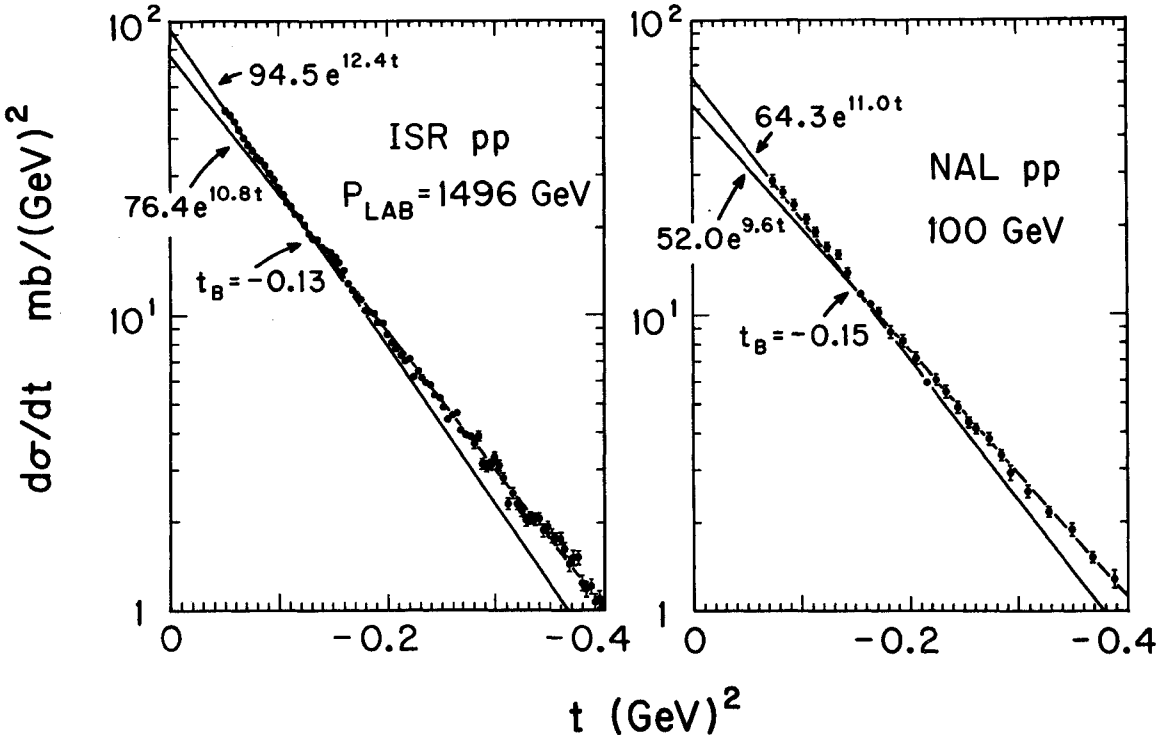

Figure 7: Comparison of the shape of NAL $d\sigma/dt$ (pp) data[20] with geometrical scaling expectations based on the ISR data.[17]

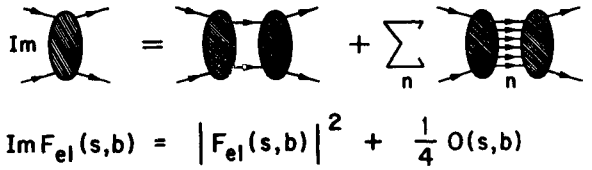

Figure 8: s-channel unitarity and inelastic overlap function O(s,b).

The pp experimental values in the ISR range are remarkably close to these numbers. The trends of similar ratios for πN and KN scattering are not well established, but the data are clearly not approaching the Van Hove limits. The B/σ_t ratios from preliminary NAL elastic scattering data[20] for slopes in the t-range $0.07 \lesssim |t| \lesssim 0.25$, are

B/σ_t(100 GeV)	pp	$\bar{p}p$	π^+p	π^-p	K^+p	K^-p
	0.282	0.282	0.370	0.372	0.376	0.443

The large t structure of $d\sigma/dt$ is sensitive to the detailed shape of S(b) at small b. The small t slope of $\ell n\, d\sigma/dt$ and the rise of σ_t with energy are correlated with the behaviour of S(b) at large b.

Although a Gaussian may be a reasonable first approximation to the pp overlap function, it has definite limitations:

(i) A small correction term which produces a flattening (relative to the Gaussian) of the overlap function at small b must be introduced to describe the dip structure of $d\sigma/dt$ at large t. Henzi and Valin proposed a simple modification of the form[22,18]

$$O(s,b) = 0.94\, e^{-b^2/R^2} + 0.54\, \left(\frac{b^2}{R^2}\right) e^{-2.6\, b^2/R^2},$$

in order to fit the $d\sigma/dt$ data. (Figure 9).

(ii) The curvature of $\ell n\, d\sigma/dt$ at small t generated by the Gaussian form of O(s,b) at large b may not suffice to completely reproduce the local slope change $\Delta B \simeq 1.6$ around $t \simeq -0.13$. In other words O(s,b) has a tail at large b beyond that of the dominant Gaussian[23-25], as would be theoretically expected.

The inelastic overlap function extracted by Miettinen and Pirilä[23] from direct Fourier-Bessel transform of the $d\sigma/dt$ data at $s = 2809$ GeV^2 is shown in Fig. 10. The experimental value of $O(s,b)$ at $b = 0$ stays constant at 94% through the ISR energy range. The protons get bigger but not blacker as the energy increases.

Other recent studies have used an "unabsorbed" overlap function in descriptions of pp elastic scattering[26]. The unabsorbed overlap function O_u is defined through the unitarity relation[27]

$$\text{Im } F_{el}(b,s) = |F_{el}(b,s)|^2 + \frac{1}{4} |S_{el}(b,s)| \; O_u$$

The absorption factor $|S_{el}|$ takes into account initial state interactions between the two protons.

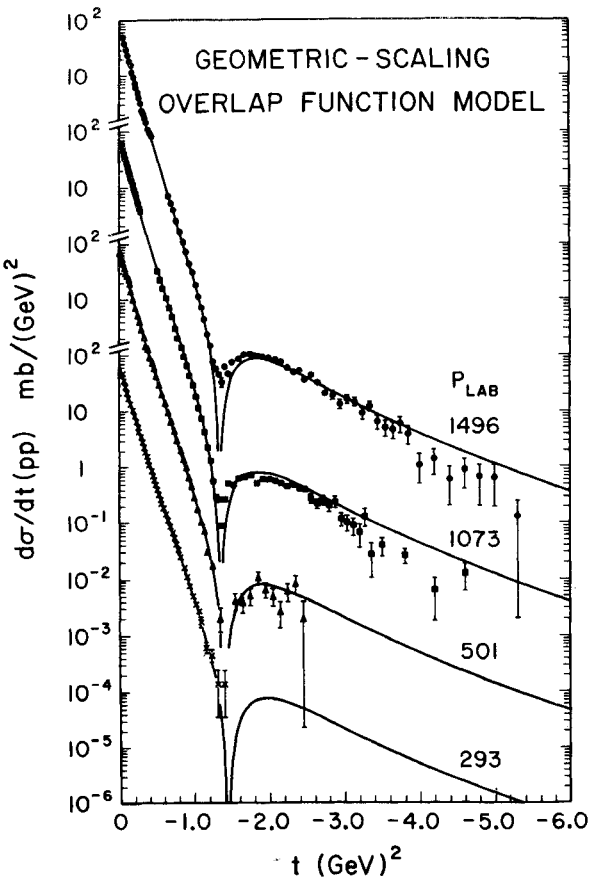

Figure 9: Inelastic overlap function description of ISR $d\sigma/dt$ (pp) data with Henzi-Valin parametrization[22] incorporating geometric scaling[18].

The unabsorbed overlap function has no unitarity bound. The unabsorbed overlap function approach is similar in spirit to eikonal models.

3. Eikonal Models

A popular alternative phenomenological approach to pp scattering has been the eikonal model. The form of the eikonal $\chi(b,s) = 2\delta(b,s)$ is the theoretical input to such descriptions. An attractive feature of the eikonal approach is that the constraints of s-channel unitarity are built in from the start: the output amplitude satsifies unitarity for any eikonal input with Im $\chi \geq 0$. Furthermore the eikonal model yields a simple picture of scattering and production processes in impact parameter. Eikonal models bear a close relation to multiperipheral models that include shadowing effects (i.e. re-scattering diagrams). The predictions of the model depend upon the form assumed for the eikonal phase.

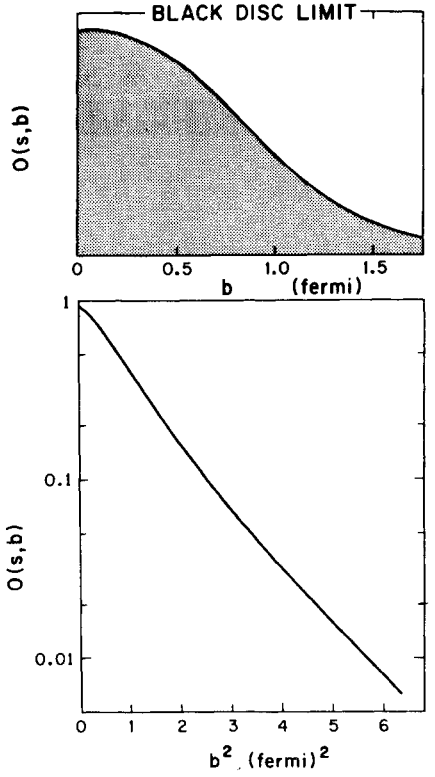

Figure 10. Inelastic overlap function found by direct Fourier-Bessel transform of $d\sigma/dt$ data at $s = 2809$ (from Ref. 23).

(a) Energy Independent Eikonal: EM Form Factor Model

Chou-Yang[28] and Durand-Lipes[29] assumed that the phase shift approaches a limiting distribution (i.e. independent of s) which is proportional to the matter density overlap $\rho(b)$ of the colliding protons,

$$\delta_1(b) = \kappa\, \rho(b)$$

where κ is an absorption coefficient. Assuming equality of matter and charge distributions

$$\rho(b) = \int_0^\infty dt\; G_E^{\,2}(t)\; J_0(b\sqrt{-t}).$$

For a dipole form factor $G_E(t) = (1 + t/\mu^2)^{-2}$, with $\mu^2 \simeq 0.71$,

$$\rho(b) \to \begin{cases} \mu^2\, e^{-\mu^2 b^2/8} & \text{at small } b \\ \mu^3(\mu b)^{5/2}\, e^{-\mu b} & \text{at large } b \end{cases}$$

Such a model predicts a diffraction dip at $t = -1.5$. Unfortunately the energy dependence of the ISR data indicates that the simplicity of this picture is not realized.

(b) Factorizable Eikonals: Asymptotic Black Disc and Modified Chou-Yang Models

In these models the phase shift is assumed to factor into a function of b times an increasing function of s[†].

$$\delta_1(s,b) = \kappa(s)\, \rho(b)$$

With a factorizable eikonal the elastic slope B from the Born amplitude is energy independent. Any shrinkage of the full amplitude must therefore be generated through the eikonal unitarization.

In modified Chou-Yang model $\rho(b)$ is determined by the EM form factor and the absorption coefficient $\kappa(s)$ is an ad hoc energy dependent factor[31-33].

In the asymptotic black disc model of Cheng-Walker-Wu[34] an energy dependence

$$\kappa(s) = s^c \qquad (c = 0.08)$$

is motivated from multiple "tower" exchange graphs of quantum electrodynamics. Their assumed form for $\rho(b)$

$$\rho(b) = f\, e^{-\lambda\{b^2 + b_o^{\,2}\}^{1/2}}$$

is designed to approach a Yukawa interaction at large b. The physical picture at asymptotic energies is an expanding black core $R_c^{\,2} \sim \ell n^2\, s$ with a constant grey fringe.

Present phenomenological fits to $d\sigma/dt$ data with these factorizable models still leave much to be desired. For example the prediction of the energy dependence of the elastic slope B is too flat for comfort over the ISR energy range. Moreover geometrical scaling is badly violated.

With the factorizable assumption two general distinctive predictions are obtained:

(i) There is little shrinkage ($\lesssim 3\%$) and σ_{el}/σ_T and σ_T/B increase by about 7% over the ISR range[††]. (Figure 11). Appreciable shrinkage cannot be generated from the eikonalization.

(ii) The height of the secondary maximum in $d\sigma/dt$ increases by at least a factor of 2 over the ISR range[32-33]. (Figure 12).

There is no indication in present data at small t for the energy dependences predicted by factorized eikonals.

[†] A more promising phenomenological possibility is an eikonal which geometrically scales. For example in the form factor model both μ^2 and κ would be s-dependent: $\mu^{-2} = 0.81 + 0.07\ \ell n\ s$, $\kappa = c/\mu^2$. Of course with such a modification there is no longer a connection with the mass in the em dipole form factor. (cf. Ref. 30).

[††] Using an energy dependence s^c for an unabsorbed inelastic overlap function Chiu-Gleiser-Wang (Ref. 35) obtain predictions for the energy dependences of B and σ_t that are very similar to the results of Cheng-Walker-Wu.

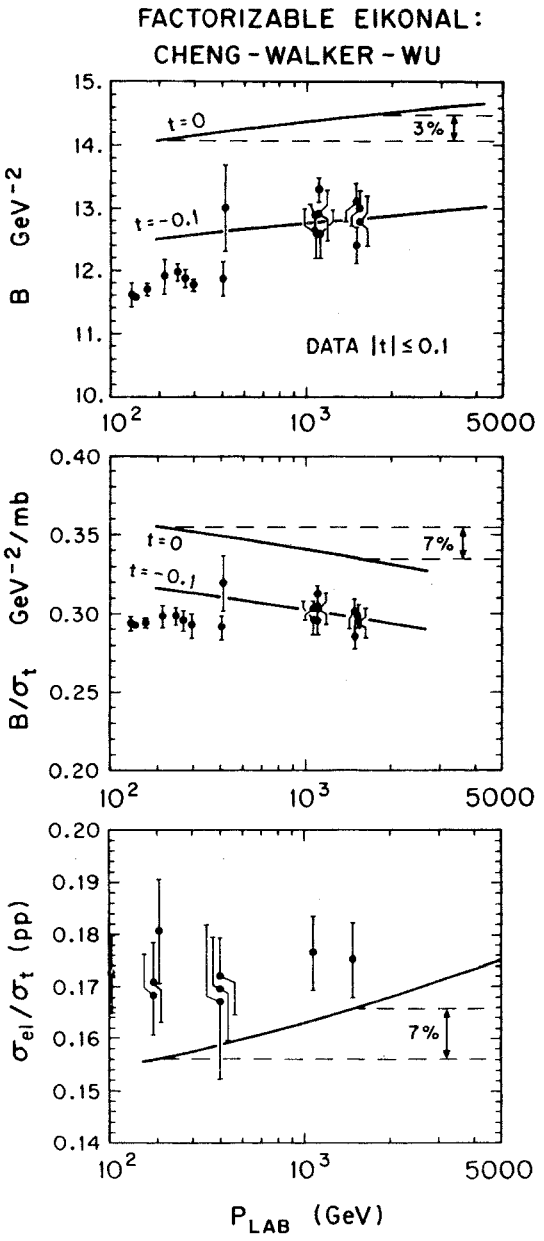

Figure 11. Predicted energy dependences of B, σ_{el}/σ_t, and σ_t/B for pp scattering for the Cheng-Walker-Wu factorizable eikonal (from Ref. 34).

The asymptotic growth with energy of the Cheng-Wu eikonal leads to an asymptotic black disc picture of the proton with

$$\frac{\sigma_{el}}{\sigma_t} \to \frac{1}{2}, \quad \frac{B}{\sigma_t} \to 0.1, \quad \sigma_t \to \ell n^2\, s, \quad \frac{\sigma_t(\pi p)}{\sigma_t(pp)} \to 1,$$

$$\frac{(d\sigma/dt)_{\text{secondary maximum}}}{(d\sigma/dt)_{t=0}} \to 1.7 \times 10^{-2}$$

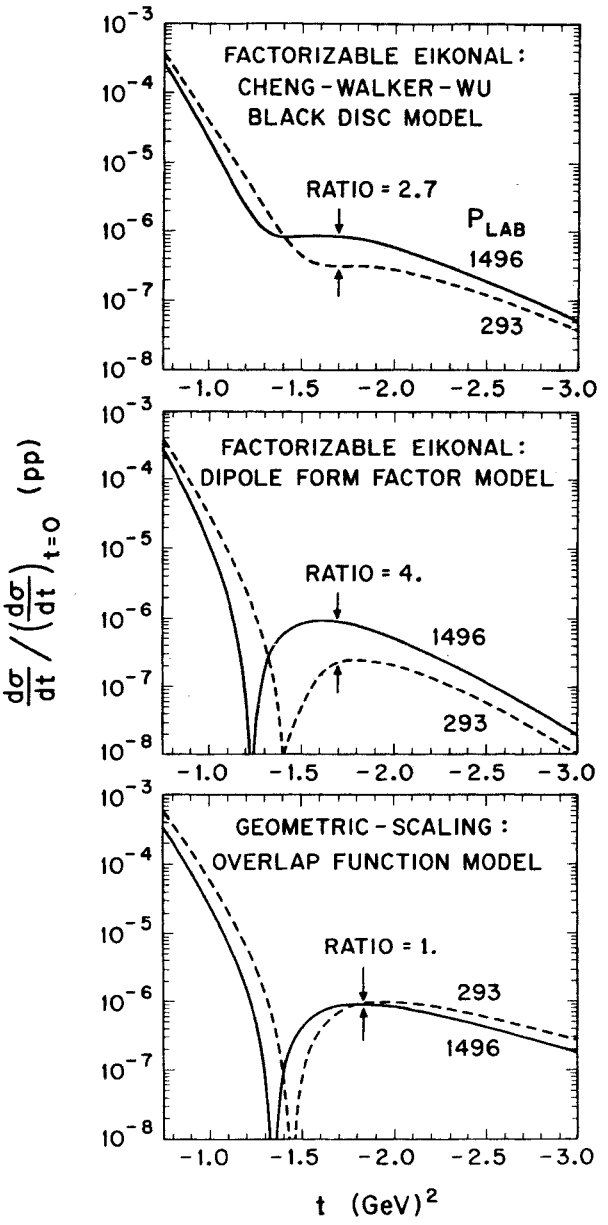

Figure 12: Characteristic predicted rise with energy of the secondary maximum of dσ/dt in factorizable eikonal models, compared with the energy independent prediction of geometrical scaling.

Since the corresponding ISR data on the ratios are far from these asymptotic limits, the theoretical energy dependence of the model seems to have little connection with data at ISR energies.

Numerous other eikonal inputs are theoretical possibilities, such as a Regge pole with $\alpha > 1$[36-38], a Regge dipole, and so forth.

(c) Naive Geometrical Pomeron

In a simple geometrical approach, Kane[39-40] represents pp diffractive elastic scattering by a black core of radius $R_c \sim \frac{1}{2}$ F and a smoothed edge of radius $R_e \sim 1$ F. His parameterization of the elastic amplitude is

$$F_{el}(s,t) = i\{A_c\, e^{B_c t}\, \frac{J_1(R_c\sqrt{-t})}{R_c\sqrt{-t}} + A_e\, e^{B_e t}\, J_o(R_e\sqrt{-t})\}$$

with a growing radius for the fringe given by

$$R_e^2(s) = R_o^2\, \ell n(-is)$$

To produce a rising σ_t, the edge strength A_e is taken proportional to R_e^2. This parameterization exhibits the qualitative features of the pp data for $|t| < 2$. The curvature of $d\sigma/dt$ at small t arises from the peripheral term and the dip at $t = -1.4$ comes mainly from the central term.

A plausible theoretical origin of the peripheral term the two pion exchange contribution to the pp elastic amplitude[41-43]. Production processes which involve pion exchange at large b cause a rise in σ_t and an increase in the elastic slope B_o at high energies. However present estimates of the magnitude of the rise in σ_t are a factor of 2 smaller than the observed rise at the ISR and the calculated energy dependence is much too gradual.

4. Experimental Tests of Models

Fortunately further precise measurements of the trends in the energy dependences of pp $d\sigma/dt$ and σ_t data through the NAL-ISR energy range will distinguish among the general classes of models, as summarized in the table below. For example, it will be possible to determine whether a nearly energy independent forward diffraction slope and a rising secondary maximum over the 100-1500 GeV range are tenable. The extent to which geometrical scaling continues to hold and the s-dependence of the radius are matters of major interest.

	σ_t	σ_{el}/σ_t	B/σ_t	$\frac{(d\sigma/dt)_{\text{secondary maximum}}}{(d\sigma/dt)_{t=0}}$
Geometrical Scaling	$R^2(s)$	constant	constant	constant
Cheng-Walker-Wu Asymptotic Black Disc Model	$\to \ell n^2 s$	increases (by 7%) $\to 1/2$	decreases (by 7%) $\to 0.1$	increases (by factor >2) $\to 1.7 \times 10^{-2}$
Regge Poles and Cuts (with $\alpha_p(0) = 1$)	rises to a constant	decreases $\to 0$	increases $\to \infty$	decreases or constant
Factorizable Eikonal	arbitrary	increases (by 7%)	decreases	increases (by factor >2)

V. SYMMETRY PREDICTIONS FOR EXCHANGE COUPLINGS

A. Total Cross Sections: SU(3) and Universality

Total cross section data at NAL energies[44] provide a new opportunity for evaluation of symmetry predictions and energy dependences of exchange amplitudes. The comparison of predictions with experiment is most straightforward for particle-antiparticle total cross section differences

$$\Delta(A^{\mp}N) \equiv \sigma_t(A^-N) - \sigma_t(A^+N)$$

where only ρ and ω exchanges are involved (ϕ exchange is decoupled from nucleons). For Regge pole exchange, power law dependences on s are expected

$$\Delta\sigma = \beta\, s^{\alpha-1}$$

Above 12 GeV the $\Delta\sigma$ data[44-46] for all reactions are approximately consistent with a single power given by

$$\alpha = 0.45$$

(Figure 13). The agreement is somewhat marginal for $\Delta(\pi^{\mp}p)$ where the trends of the data from different accelerators appear to be inconsistent. A slightly higher value of α_ρ might be better for the $\Delta(\pi^{\mp}p)$ data. Nevertheless, for the present purpose of symmetry tests, a more detailed description of the Δ's allowing for different ρ and ω intercepts is unnecessary.† The $s^{-0.55}$ power law coefficients for this fit to the data are given below.

	β	exchange
$\Delta(p^{\mp}p)$	69.6	ω,ρ
$\Delta(K^{\mp}p)$	27.1	ω,ρ
$\Delta(\pi^{\mp}p)$	12.4	ρ
$\Delta(p^{\mp}D)$	174.5	ω
$\Delta(K^{\mp}D)$	56.4	ω
$\Delta(p^{\mp}n)$	61.2	ω,ρ
$\Delta(K^{\mp}n)$	12.9	ω,ρ

We use these coefficients in evaluating the various symmetry relations.

The assumption of SU(3) and universality for the couplings of the ρ and ω exchanges leads to a series of relations among total cross section differences. (The assumption that the ρ and ω exchanges are coupled to conserved currents leads to universal couplings). Comparisons of the relations with experiment are made in the following table by taking the ratios of the β's from the power law fit to the data.

Prediction	Experiment	Derivation
$\frac{\Delta(p^{\mp}D)}{\Delta(K^{\mp}D)} = 3$	3.1	ω - universality
(Levinson-Lipkin-Wall)		
$\frac{\Delta(K^{\mp}p)}{\Delta(\pi^{\mp}n)} = 2$	2.2	ρ,ω - universality
$\frac{\Delta(K^{\mp}p)}{\Delta(K^{\mp}n)} = 2$	2.1	
(Johnson-Treiman)		
$\frac{\Delta(p^{\mp}p)}{\Delta(\pi^{\mp}p)} = 5$	5.6	ρ,ω - universality
$\frac{\Delta(p^{\mp}p)}{\Delta(p^{\mp}n)} = \frac{5}{4}$	1.14	
(Freund)		
$\frac{\Delta(K^{\mp}p) - \Delta(K^{\mp}n)}{\Delta(\pi^{\mp}p)} = 1$	1.14	ρ - SU(3)
(Barger-Rubin)		

The overall agreement of these symmetry relations with experiment is impressive. The ρ-universality relations are in better accord with experiment than was first inferred from data at BNL energies.

The sums of particle-antiparticle total cross sections (Figure 14)

† An evaluation of the symmetry relations using non-degenerate ρ and ω trajectory intercepts is given by R E Heindrick, P Langacker, S J Orfanidis, V Rittenberg, and B E Lautrup, conference paper 1097.

$$\Sigma(A^{\mp}p) \equiv \sigma_t(A^-p) + \sigma_t(A^+p)$$

isolate even signature exchanges, the Pomeron and the f^0. Unfortunately, since these exchanges have the same quantum numbers, further separation of the Pomeron and f^0 contributions can only be made on the basis of assumptions about energy dependence. Without a theoretical basis for the energy dependence of the Pomeron amplitude, phenomenological fits to the Σ's are not very illuminating. The ratio of

$$\frac{\Sigma(NN)}{\Sigma(\pi N)} = 1.68$$

at the highest energy, 200 GeV, is only ∼10% greater than the quark counting ratio of 3/2. (Figure 15). The value of the ratio

$$\frac{\Sigma(\pi N)}{\Sigma(KN)} = 1.17$$

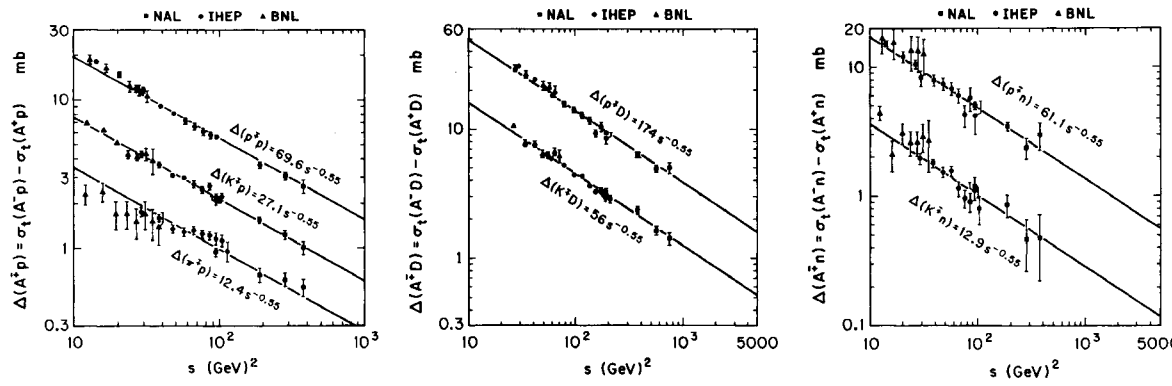

Figure 13: Power law dependences of particle-antiparticle total cross section differences.[44-46]

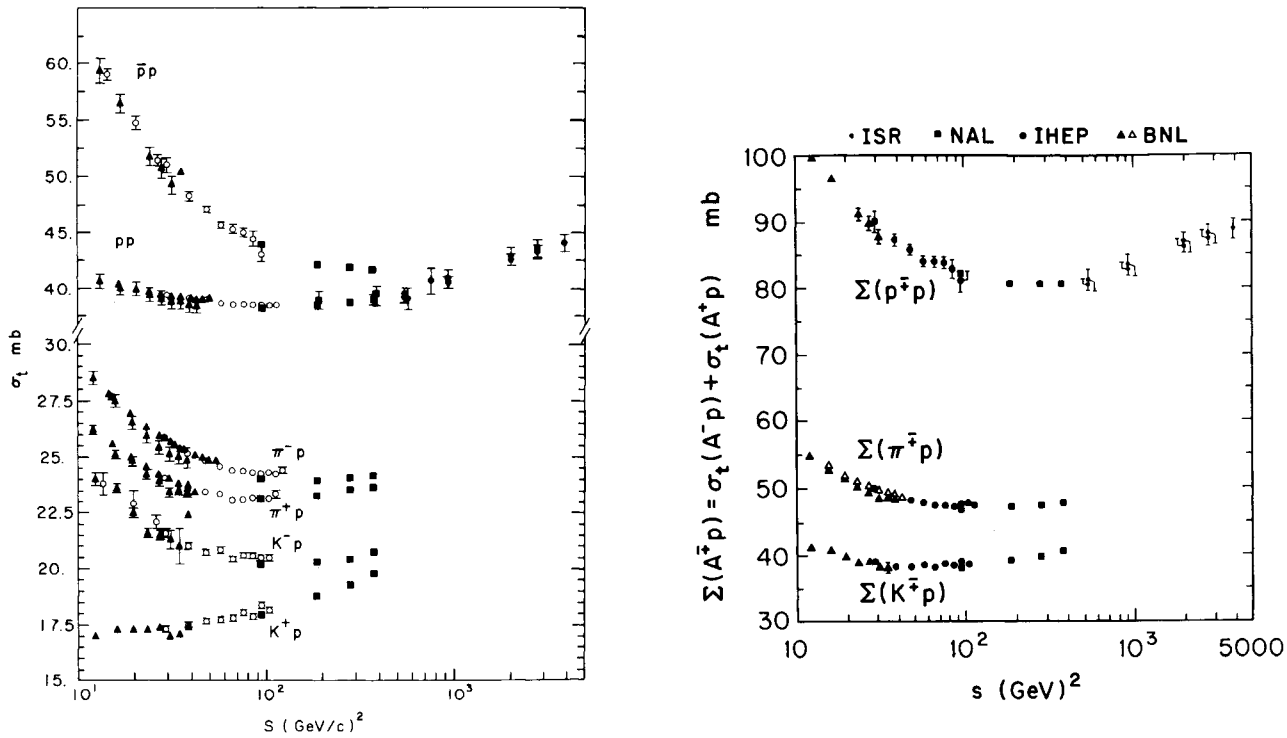

Figure 14: Data on total cross sections[44-46] and particle-antiparticle sums.

at 200 GeV continues to suggest probable asymptotic symmetry breaking for the unitary singlet Pomeron couplings.

In order to try to restore quark counting ratios of 1:1:3/2 for the Pomeron coupling to pions, kaons, and nucleons, Lipkin[48] introduced a Pomeron-Regge double scattering component in addition to Pomeron and Regge exchanges. The strength of this Pomeron-Reggeon cut was assumed to be proportional to the product of the quark counting strengths for single Pomeron and single Regge exchange. From this 3-component model Lipkin obtained the sum rule,

$$\sigma_t(\pi^- D) - \sigma_t(K^- D) = \frac{1}{3}\sigma_t(pD) - \frac{1}{2}\sigma_t(K^+ D).$$

Lower energy data agree with this relation but deviations occur at IHEP and NAL energies. (Figure 16). In any case two aspects of the model would be difficult to understand in terms of conventional cut models:

(i) The cut contributions in the model can be determined from total cross sections by algebraic relations. The resulting Pomeron $-f^0$ cut has an empirical $s^{-0.13}$ energy dependence. However the energy dependence of the $P-f^0$ cut should be no slower than the f^0 pole, which has a $s^{-0.5}$ behaviour.

(ii) In conventional models the cut is a convolution. This introduces a dependence of the cut strength on the t-dependence of the Pomeron and Regge exchanges. It is experimentally untrue that the t-dependence of the Pomeron is universal in πN, KN, and NN which would be required by the calculational recipe used in relating the cut contributions in different reactions.

B. SU(3) for Production Amplitudes

Relations among differential cross sections based on SU(3) for the couplings of t-channel exchanges work surprisingly well above 5 GeV. The first such SU(3) test was a sum rule for the ρ, A_2 charge exchange reactions[49]

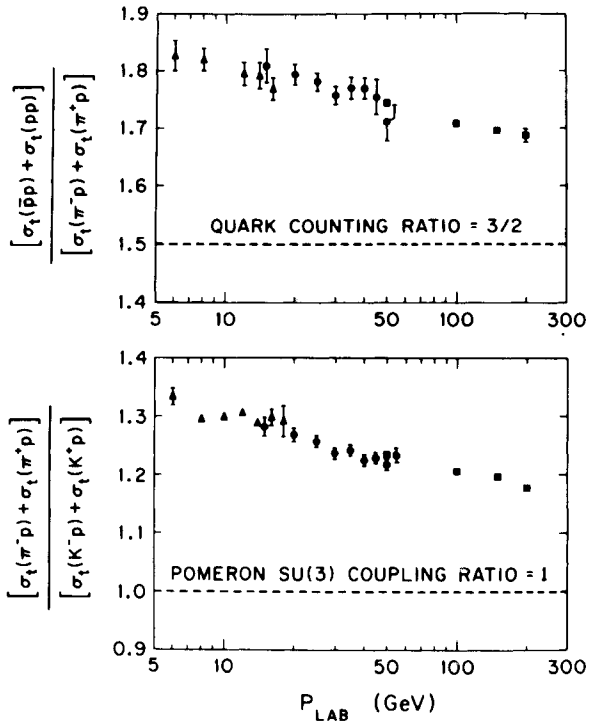

Figure 15: Comparison of total cross section data with (a) the quark counting prediction $\Sigma(NN)/\Sigma(\pi N) = 3/2$ and (b) the unbroken SU(3) prediction $\Sigma(\pi N)/\Sigma(KN) = 1$.

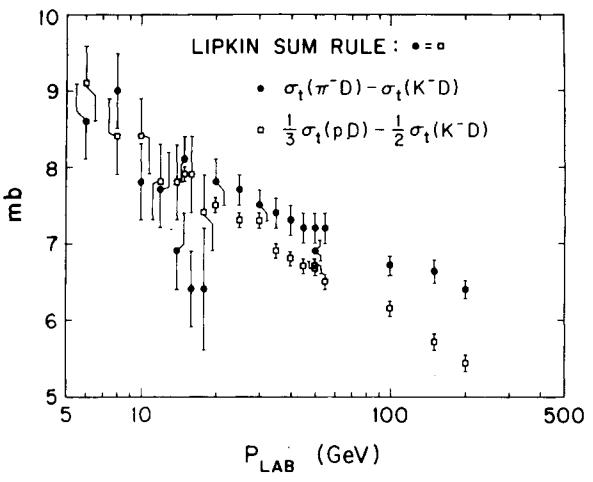

Figure 16: Evaluation of the Lipkin sum rule[48] based on a 3-component picture (Pomeron, Regge, Pomeron-Regge cuts).

$$\frac{d\sigma}{dt}(\pi^- p \to \pi^0 n) + 3\frac{d\sigma}{dt}(\pi^- p \to \eta^0 n) = \frac{d\sigma}{dt}(K^- p \to \bar{K}^0 n) + \frac{d\sigma}{dt}(K^+ n \to K^0 p)$$

A new experimental comparison at 6 GeV using recent Argonne KN charge exchange data[50] shows reasonable agreement. (Figure 17). At lower energies, where line reversal breaking of $K^- p \to \bar{K}^0 n$ and $K^+ n \to K^0 p$ cross sections is substantial, violations of the sum rule are found[51].

The success of the SU(3) charge exchange sum rule was often interpreted as evidence for relatively small absorptive corrections in the dominant helicity flip amplitudes[52†]. However more recent evidence from vector meson production reactions[54] indicates that SU(3) holds for both flip and non-flip amplitudes. The SU(3) sum rule for the vector meson production cross sections on nucleons is

$$\rho\frac{d\sigma}{dt}(\pi^- p \to \rho^0 n) + \rho\frac{d\sigma}{dt}(\pi^- p \to \omega^0 n) = \rho\frac{d\sigma}{dt}(K^- p \to \bar{K}^{0*} n) + \rho\frac{d\sigma}{dt}(K^+ n \to K^{*0} p)$$

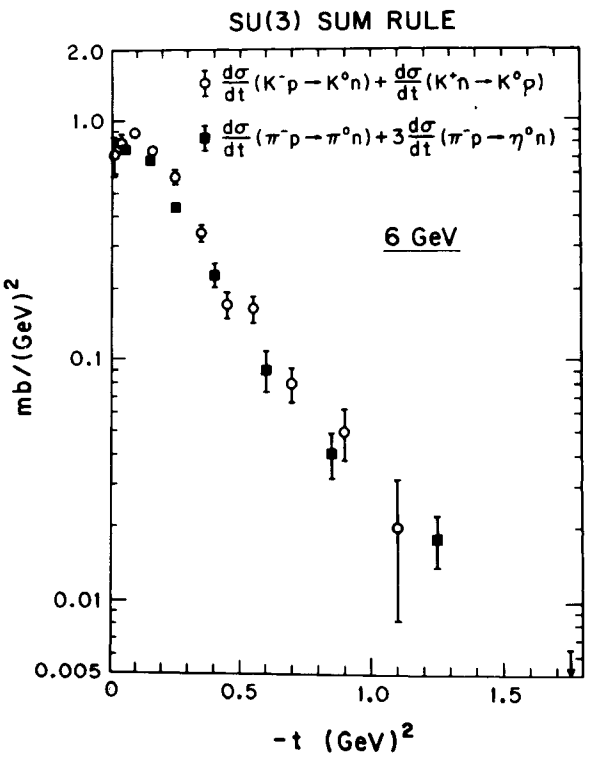

Figure 17: Evaluation of SU(3) sum rule for charge exchange reactions at 6 GeV.

where ρ is any density matrix element. An experimental comparison with this relation for both unnatural parity (π, B) and natural parity (ρ, A_2) exchange contributions is shown in Figure 18, using new Argonne K* data at 6 GeV[55].

Another verification of SU(3) for exchanges are the amplitude equalities[56]

$$A(K^- p \to \phi\Lambda) = A(\pi^- p \to K^{*0}\Lambda)$$

which are in beautiful accord with data at 4 GeV[57]. Couplings of t-channel exchanges which respect SU(3) for both helicity non-flip and flip amplitudes also explains several approximate experimental polarization equalities in hypercharge exchange reactions[57,58]:

$$P(K^- p \to \pi^0\Lambda) \simeq -P(K^- p \to \pi^-\Sigma^+)$$

$$P(\pi^- p \to K^0\Lambda) \simeq -P(\pi^+ p \to K^+\Sigma^+)$$

$$P_n(K^- p \to \omega\Lambda) \simeq -P_n(K^- p \to \phi\Lambda)$$

† The polarized cross sections will satisfy a similar sum rule if the non-flip couplings of the exchanges also respect SU(3). Existing measurements for π^0, η, and $\bar{K}$ reactions yield a prediction of a positive polarization in $K^+ n \to K^0 p$. (Ref. 53).

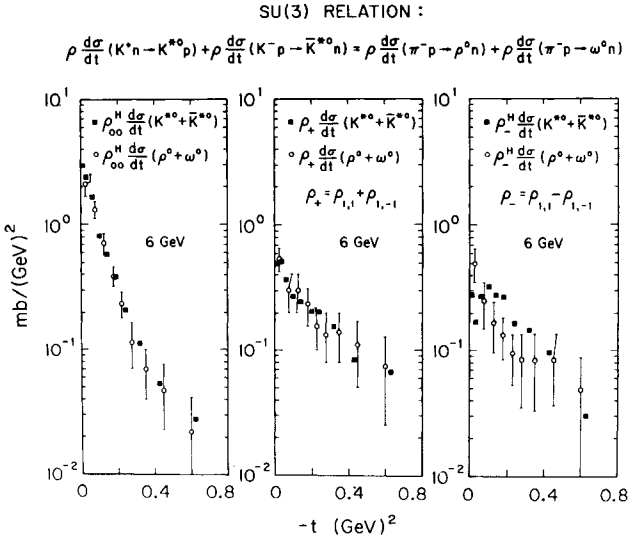

Figure 18: Experimental comparison of SU(3) relation for vector meson production cross sections (figure by R D Field).

(P_n is the polarization arising from the interference between the natural parity vector-tensor exchange amplitudes.)

There are numerous possibilities for further correlations of data on different reactions through SU(3) or quark model couplings. For example, the quark model relates the density matrix elements of $pp \to n\Delta^{++}$ and $K^+n \to K^{*o}p$ reactions [56,59]. New Argonne data at 6 GeV show that this relation is also well satisfied. (Figure 19)

The success of these various comparisons suggest that SU(3) predictions for exchanges may work to an accuracy of 10-20% at high energy, for all helicity amplitudes.

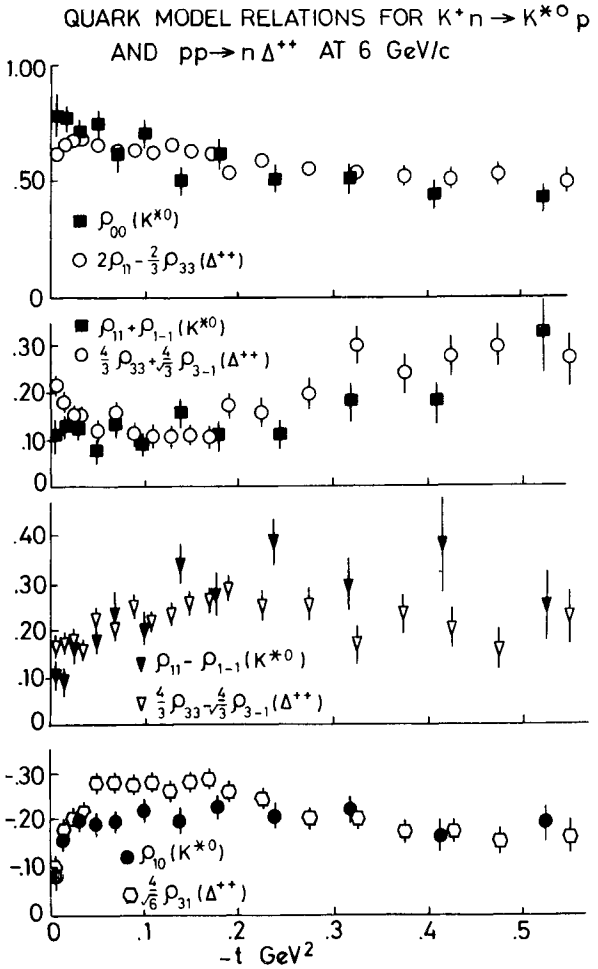

Figure 19: Quark model correlation[59] of data on $pp \to n\Delta^{++}$ and $K^+n \to K^{*o}p$ reactions[55].

VI πN CHARGE EXCHANGE REACTIONS

The Serpukhov[60] and NAL[61] data on $\pi^-p \to \pi^o n$ and $\pi^-p \to \eta^o n$ cross sections will provide a strong constraint on exchange mechanisms. Since the results of the NAL experiment on π^o and η^o at 20, 40, 65 and 100 GeV and the new IHEP results on η^o at 40 GeV became available for the first time at this conference, the implications of these data are still largely unexplored. The following represents a summary of preliminary deductions based on the new data.

The NAL and IHEP experiments provide a long lever arm for determining whether the differential cross sections can be described in terms of single Regge pole exchange. When full systematic errors are taken into account, the charge exchange data at fixed t are consistent with the Regge pole expectation of a linear dependence of ℓn $d\sigma/dt$ on ℓn s:

$$\ell n \frac{d\sigma}{dt} = (2\alpha(t)-2)\ell n\, s + \ell n\, \beta(t)$$

The trajectory determinations are precise only when the 20-100 GeV data are considered in conjunction with the earlier CERN measurements[62] below 20 GeV. More importantly, trajectory determinations for the interesting region $|t| > 0.5$ GeV^2 are possible only if the data below 20 GeV are simultaneously considered. To avoid the question of a normalization difference between NAL and IHEP data, these experiments can be separately used with the CERN data in making trajectory determinations. The slope of a trajectory is determined by the shrinkage of $(d\sigma/dt)/(d\sigma/dt)_{t=o}$ which is less dependent on experimental normalizations than the intercept. All high energy experiments show a comparable amount of shrinkage with increasing energy.

The energy dependence and shrinkage of $d\sigma/dt(\pi^-p \to \pi^o n)$ up to 100 GeV are characterized by an approximately linear trajectory

$\alpha_\rho(t) = 0.53 + 0.83t$

[Figure 20]. The apparent anomalous behaviour in the effective ρ trajectory determination at very small t-values is probably not real.+ The absence of any anomalous energy dependence in the region of the dip in $d\sigma/dt$ at $t \simeq -0.55$ GeV^2 indicates that the helicity flip and non-flip amplitudes have similar energy dependences. In a ρ-Regge exchange model

$$s^{-[2\alpha_\rho(t)-2]} \frac{d\sigma}{dt} = \beta(t)$$

Such a comparison is made in Figure 21, where it is observed that the 5.9 and 100 GeV data fall on a universal (i.e. s-independent) curve.

The intercept $\alpha_\rho(0) = 0.53$ from the above trajectory is close to the ρ-trajectory intercept determined from (i) the energy dependence of the NAL data[14] on $[\sigma_t(\pi^- p) - \sigma_t(\pi^+ p)]$ and (ii) similar analysis of IHEP and CERN $\pi^- p \to \pi^0 n$ data. The turnover of $d\sigma/dt$ near $t = 0$ is determined more precisely by the NAL data than by previous experiments. This turnover pins down the ratio of helicity amplitudes at small t. A refit of a ρ-exchange model to the NAL $\pi^- p \to \pi^0 n$ data by R. Field gave an 8% larger ratio of helicity flip to non-flip amplitudes at small t. Such an increase in this ratio is also compatible with the lower energy CERN measurements.

From IHEP-CERN data[60,62] on $\pi^- p \to \eta^0 n$ for $3 \lesssim p_{LAB} \lesssim 40$ GeV we now have the first indication that the A_2 trajectory may also fall linearly at large t [Figure 22]. Previously the data below 20 GeV seemed to indicate a tendency for the A_2 trajectory to flatten out in the vicinity of $\alpha = 0$ at large t. A linear interpolation of the IHEP-CERN A_2 trajectory determinations out to $t = -1.2$ gives

$\alpha(t) = 0.45 + 0.7t$

This is also reasonably consistent with A_2 trajectory values based on NAL and CERN data.

The experimental ρ and A_2 trajectories are definitely not exchange degenerate at small t. The non-degeneracy is clearly evident in the energy dependence of the ratio of $\pi^- p \to \pi^0 n$ to $\pi^- p \to \eta^0 n$ differential cross sections [Figure 23]. The trajectory splitting is

$\alpha_\rho(0) - \alpha_{A_2}(0) \simeq 0.1$

The slope of the A_2 trajectory is smaller than that of the ρ and the two trajectories cross at $t \simeq -0.5$.

In summary, the dominant features of the charge exchange reactions can be simply described by the Regge pole model up to the highest available energies. The qualitative features of the new data are far simpler than anticipated in some models. A reproduction of the observed energy dependences of vector and tensor exchange amplitudes is an important test of phenomenological models, as will be discussed more fully in the next section.

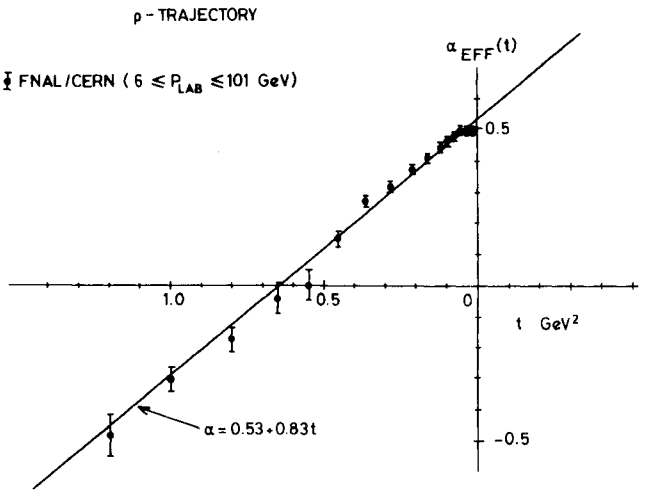

Figure 20: ρ- trajectory from $\pi^- p \to \pi^0 n$ based on NAL and CERN data. (trajectory determinations are from Ref. 61.).

+J. Mellema (private communication)

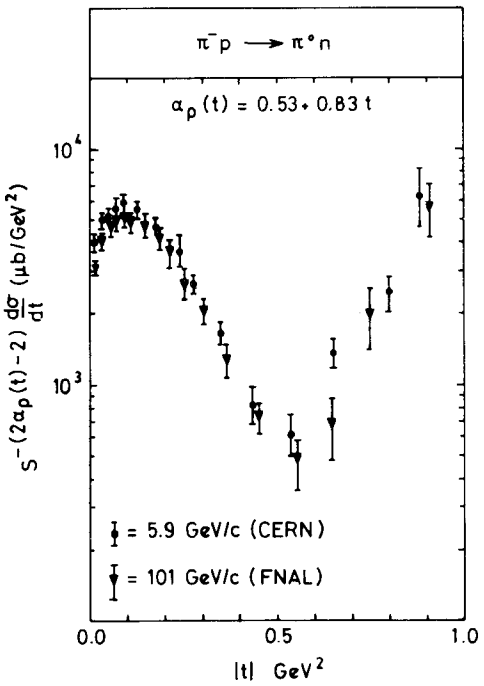

Figure 21: Plot of $s^{-(2\alpha_\alpha(t)-2)} d\sigma/dt(\pi^- p \to \pi^0 n)$ at 5.9 and 100 GeV, using $\alpha_\rho(t)=0.53 + 0.83t$.

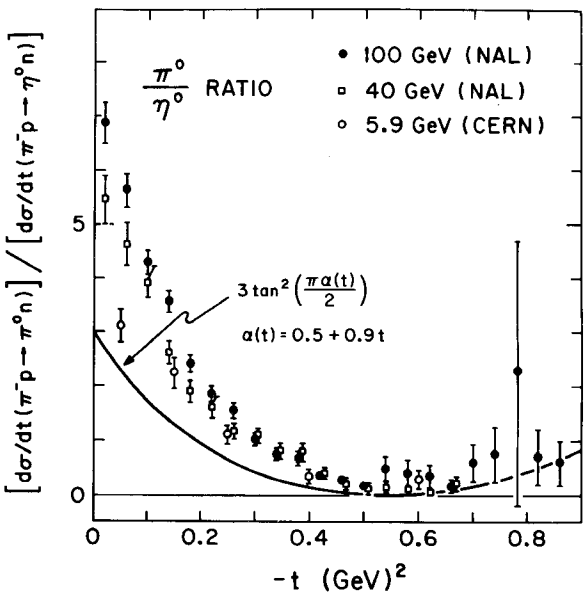

Figure 23: Ratio of $\pi^- p \to \pi^0 n$ and $\pi^- p \to \eta^0 n$ differential cross sections at 5,9,40 and 100 GeV. (figure prepared by R Field).

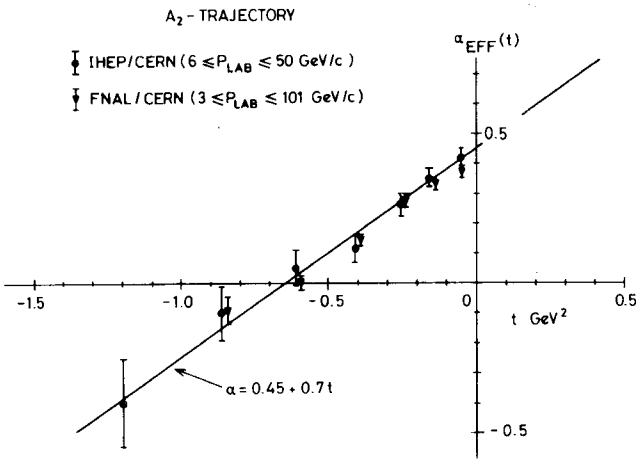

Figure 22: A_2 trajectory from $\pi^- p \to \eta^0 n$ based on NAL/CERN and IHEP/CERN data (trajectory determinations from Refs. 60,61).

VII PHENOMENOLOGY OF INELASTIC REACTIONS: STATE OF THE ART

In the absence of a real theory of two body hadron scattering, several different languages have been developed to describe the features of inelastic scattering data for near forward or near backward scattering angles.[63] All these approaches are based on the qualitatively well established notion of particle exchange. Generally, the Regge pole framework is invoked at some stage, for t-channel exchanges or for s-channel resonances. Since there exists a considerable amount of flexibility in each approach, it is often difficult to single out definitive experimental tests. Evaluations of how successful the various approaches are in describing scattering data is a somewhat subjective matter and it is unlikely that concensus of opinion could be reached at present. The following reflects my personal assessment of strong points and limitations of models of major current interest.

A. Regge Pole Exchange

The success of the Regge pole idea has been in correlating energy dependences of differential

cross sections with trajectories $\alpha(t)$ determined by extrapolations in a Chew-Frautschi plot of particle states

$$\frac{d\sigma}{dt} \propto s^{2\alpha(t)-2}$$

At $t = 0$ (or $u = 0$) such correlations hold remarkably well, but they sometimes meet with mixed success for $t < 0$.

The model suffers embarrassments such as the predicted vanishing of π exchange at $t' = 0$ and the empirically observed $J_0(R\sqrt{-t})$ structure of the zeros of helicity non-flip vector exchange amplitudes. In spite of such problems pole models have been effectively used in making quantitative fits to scattering data and FESR. In this sense the pole model serves a very useful role as the high energy equivalent of a phase shift analysis. Unlike phase shifts, pole models can often be extrapolated beyond the regions where the fits are made. As a case in point, Figure 24 compares recent $\pi^- p \to \pi^- p$ forward elastic data from Serpukhov[64] and NAL[20] with extrapolations of a 5 pole fit[65] made 5 years ago to the then existing data below 30 GeV.

B. Reggeized Absorption Approach

The absorption model is based on the plausible argument that initial and final state rescattering effects are important in determining the t-dependent structure of hadron scattering cross sections. The input Born exchange amplitude is a Regge pole. In impact parameter the fundamental equation of the linear absorption model is

$$A(s,b) = R(s,b)\, S_{eff}(s,b)$$
$$= R(s,b)[1 + i\, M_{eff}(s,b)]$$

where R is the Regge pole input, S_{eff} is the effective elastic rescattering S-matrix, and A is the output amplitude. Detailed assumptions about R and S_{eff} have evolved considerably from those of early absorption model calculations. The most essential changes which have been made are:-

(i) A substantial negative real part for $t \neq 0$ and shrinkage is necessary in the effective rescattering amplitude.[40] Earlier applications used a pure imaginary rescattering amplitude with no shrinkage.

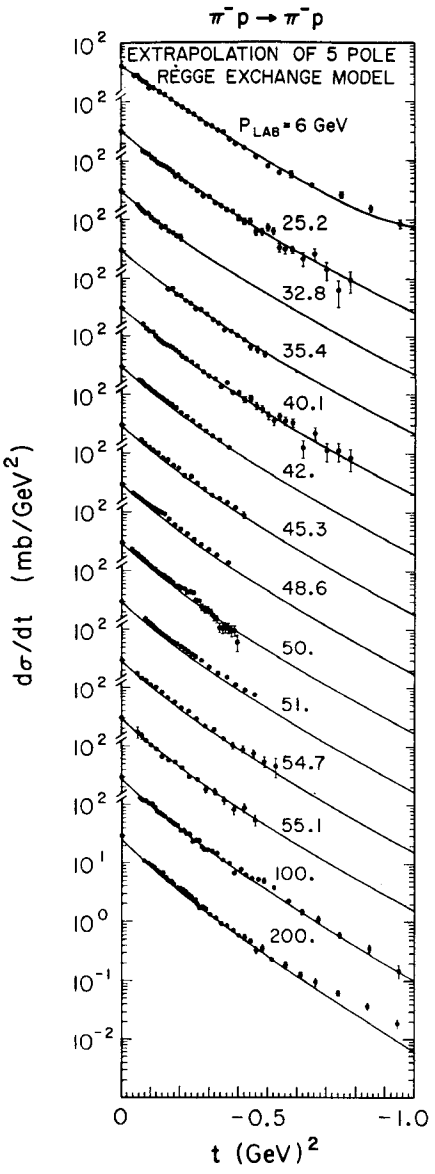

Figure 24: Extrapolations of Barger-Phillips 5-pole model[65] compared with IHEP[64] and NAL[20] $\pi^- p$ elastic data.

(ii) Input Regge pole residues with t-dependence are needed for consistency with FESR.[66] Previously, constant input pole residues were advocated.

All Regge-Regge rescattering contributions are neglected. The most comprehensive recent absorption model investigations are those of Hartley-Kane,[40] Bali-Dash,[67] and Field-Sidhu.[68] Although the assumed forms for the rescattering amplitudes differ,† similar results were obtained in global fits to pseudoscalar meson-baryon scattering data at small t.††

Some notable success of the new absorption model are:

(i) The effective shrinkage of the cut term approximates that of the pole below 20 GeV.

(ii) Qualitative agreement is achieved with the observed line reversal breaking in cross sections and polarizations.†††

(iii) Problems with π exchange and non-flip amplitudes in the Regge pole model are eliminated by the absorptive cuts.

An essential requirement in the absorption model explanation of the systematics of line reversed reaction cross sections and polarizations is that input vector trajectories must lie higher than input tensor trajectories. In current analyses a splitting

$$\alpha_T(t) \simeq \alpha_V(t) - 0.2$$

of the input trajectories is used, but as a by-product $d\sigma/dt$ $(\pi^- p \to \eta^o n)$ is predicted to fall too rapidly with energy relative to $d\sigma/dt$ $(\pi^- p \to \pi^o n)$. Whether adequate line reversal breaking can still be maintained with the experimental ρ-A_2 trajectory splitting $\Delta\alpha(0) \sim 0.1$ is a quantitative question which deserves further attention. A definitive prediction of the current absorption approach is a substantial increase in line reversal breaking in cross sections from 10 to 100 GeV.

The effective shrinkage of the absorbed ρ-amplitude departs substantially at large t from the linear pole input in the 20-100 GeV range, as illustrated in Figure 25. The NAL data will test whether the new absorption model still has difficulty in generating sufficient shrinkage at large t.

C. Direct Channel Peripheral Models

A direct s-channel approach has been advocated as an alternative to the t-channel Regge approach. The dominant s-channel resonances are peripheral and the effective direct channel Regge trajectory $\alpha(s)$ interpolating the spins of these resonances is

---

†For Hartley and Kane M_{eff} = P+D where P is the naive geometrical Pomeron (cf Sec. 11) and D is a peripheral diffractive contribution $D \propto J_o(R\sqrt{-t})$. Bali and Dash absorb with a bare Pomeron pole of intercept $\alpha_p(0) = 0.85$, confining their analysis to data below 30 GeV.

††In describing vector meson production reactions, Field and Sidhu found it necessary to increase the absorption above that used by Hartley and Kane for pseudoscalar meson-baryon reactions.

†††For reactions related by line reversal, duality arguments or exchange degenerate pole models predict the amplitudes of one reaction to be real and the amplitudes of the other reaction to have the same magnitude and a rotating phase $(e^{-i\pi\alpha(t)})$, e.g.

$K^+ n \to K^o p$ (real) $\quad K^- p \to \bar{K}^o n$ (rotating)

$K^- n \to \pi^- \Lambda$ (real) $\quad \pi^- p \to K^o \Lambda$ (rotating)

Experimentally, the differential cross sections for the "real" reactions are larger than the corresponding "rotating" reactions at least for energies below $\sim$ 6 GeV.

$$\frac{\text{Re } \alpha(s) + 1/2}{k_s} \simeq R \simeq 1 \text{ Fermi}$$

where k_s is the c.m. momentum. From duality of the high energy amplitude with the peripheral resonances, an amplitude dependence

$$\text{Im } f_{\Delta\lambda} = \beta(s,t)\, J_{\Delta\lambda}(R\sqrt{-t})$$

is expected if the width Im $\alpha(s)$ is small. Here $\Delta\lambda$ is the net helicity flip. This Bessel function t-dependence is the central prediction of Harari's dual absorption model.[69] The qualitative agreement of the zero locations of $\Delta\lambda = 0$ vector exchange amplitudes ρ, ω, K_V^* with the zeros of $J_o(R\sqrt{-t})$ is striking. [Figure 26] Tensor exchange $\Delta\lambda = 0$ amplitudes A_2, f^o, K_T^{**} are more difficult to extract from experiment, but convincing evidence has accumulated that $\Delta\lambda = 0$ tensor exchanges are not peripheral in the Bessel function sense.[70] This qualitative difference of vector and tensor non-flip amplitudes remains as a basic difficulty for s-channel models which incorporate duality.

The s-channel peripheral framework has been extended by several groups[71-74] to allow a description of both real and imaginary parts of scattering amplitudes. The dominance of a single effective s-channel complex peripheral trajectory $\alpha(s)$ is assumed. The scattering amplitude is then proportional to a Hankel function

$$f_{\Delta\lambda}(s,t) = \beta(s)\, iH_{\Delta\lambda}^{(1)}\left(\frac{\alpha(s) + 1/2}{k_s}\sqrt{-t}\right)$$

At low s-values where Re $\alpha(s) \gg$ Im $\alpha(s)$, this reproduces the simple geometrical formula

$$\text{Im } f_{\Delta\lambda}(s,t) \propto J_{\Delta\lambda}(R\sqrt{-t})$$

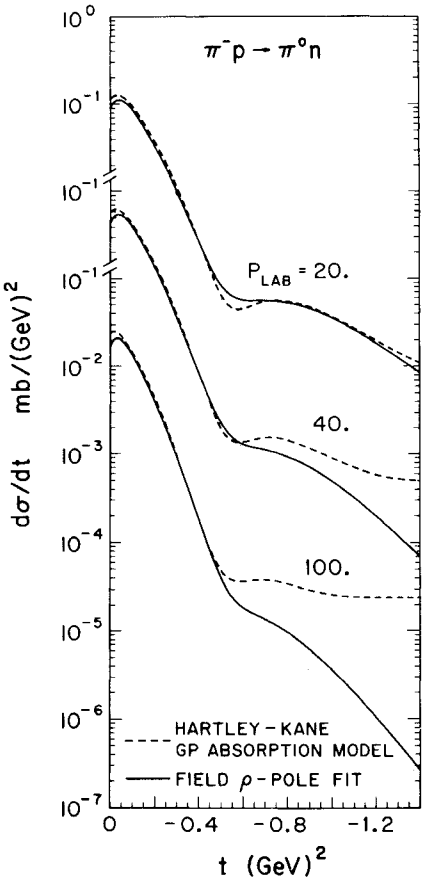

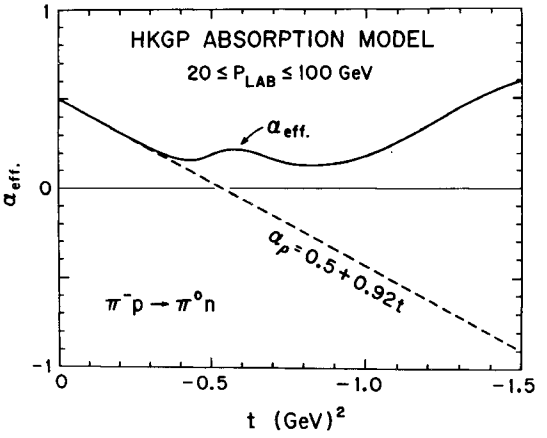

Figure 25: Energy dependence of $d\sigma/dt$ ($\pi^- p \to \eta^o n$) in the Hartley-Kane geometrical pole absorption model[66] compared with a linear ρ trajectory pole model:

a) $d\sigma/dt$ at fixed s versus t.

b) effective trajectory for $20 \lesssim P_{LAB} \lesssim 100$ GeV (Private communication from G Kane and R Field).

The Schrempps[71] assumed an s-channel trajectory of the form†

$$\alpha(s) = R\, k_s\, [1 + i(2/\pi)\, \ell n\, (s/s_o)] \quad \text{for } s > 0$$

and used a duality prescription for (s,t) and (s,u) type contributions abstracted from the Veneziano formula. Re $\alpha(s)$ determines oscillations of the amplitude in $\sqrt{-t}$ and Im $\alpha(s)$ determines the rate of shrinkage of the amplitude. For reactions with an exotic s or u channel the prediction for the t-dependence is

$$\sqrt{-t}\,\frac{d\sigma}{dt} = f(s)\, \exp\{-\sqrt{-t}\,(\frac{2\ \mathrm{Im}\ \alpha(s)}{k_s})\}$$

$$= f(s)\, \exp\{-\sqrt{-t}\,\frac{2R}{\pi}\,\ell n\,\frac{s}{s_o}\}$$

for the restricted t-range $|t| \gtrsim 0.25$.†† The data on a number of exotic channels are consistent with this exponential $\sqrt{-t}$ dependence at large t. [Figure 27]. An interesting general property of the model is an approximate derivative relationship between helicity amplitudes[71,73,74]

$$f_{\Delta\lambda=1}(s,t) \propto \frac{\partial}{\partial\sqrt{-t}}\, f_{\Delta\lambda=0}(s,t)$$

This relation is well satisfied by the $\pi^- p \to \pi^0 n$ amplitudes from the 6 GeV amplitude analysis

In impact parameter the relation is

$$f_{\Delta\lambda=1}(s,b) \propto b\, f_{\Delta\lambda=0}(s,b)$$

To proceed further, parametrizations are introduced for the unknown s-dependence of the Regge residues. With particular assumptions, the $\Delta\lambda = 1$ amplitude can be cast in the form of a t-channel Regge pole with effective trajectory

$$\alpha_{\mathrm{eff}}(t) = \alpha_o - \frac{R}{\pi}\sqrt{-t}$$

while the $\Delta\lambda = 0$ amplitude simulates a t-channel Regge cut with a considerably faster energy

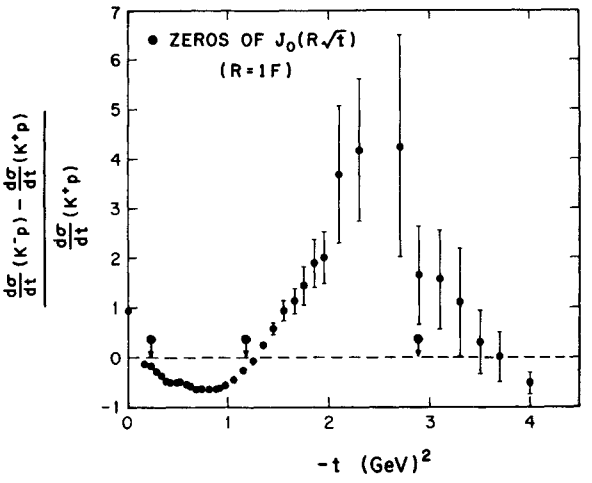

Figure 26: Bessel function structure of non-flip vector exchange amplitude in KN scattering (from A Eide, et al., Nucl.Phys. B60, 173 (1973).

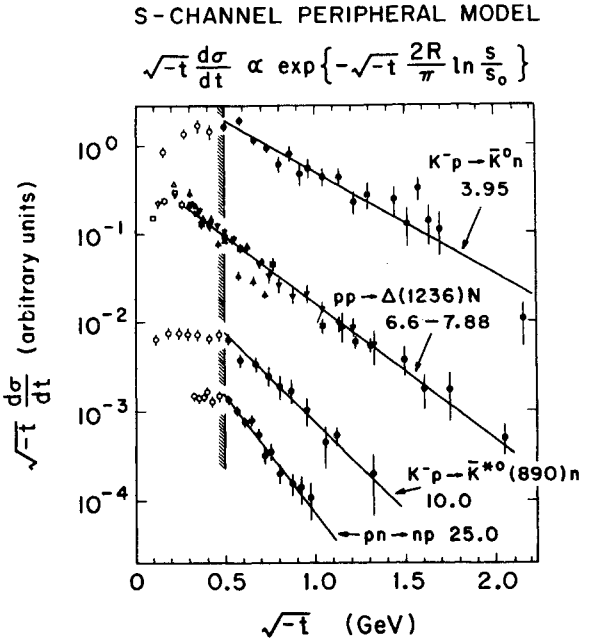

Figure 27: Comparison with data of s-channel peripheral model expectations of an experimental $\sqrt{-t}$ dependence of $d\sigma/dt$ for reactions with an exotic s or u channel. (from Ref.71).

† In descriptions of low energy $\bar{K}N$ data with a similar s-channel model, Hara et al. [Ref. 73] use a more complicated form for Im $\alpha(s)$ at low s, with this asymptotic behaviour.

†† The rigorous large J behaviour $F_J \sim e^{-m_t J/k_s}$, where m_t is the smallest mass exchanged in the t-channel, cannot be obtained from a finite number of direct channel Regge poles. Hence to apply this approach at small t, some ad hoc modification at large J is necessary. Specific prescriptions are sometimes introduced in order to apply the model at small t.

dependence than the pole at low energies. [Figure 28]. However the $\pi^- p \to \pi^0 n$ data from 3 to 100 GeV give no evidence for a different energy dependence in the dip region where the non-flip amplitude contribution dominates.

D. Dip Systematics for Tensor Exchanges

The explanation of the origin of dips in differential cross sections at fixed momentum transfers has been a focal point of interest in two body phenomenology. In addition to dips at $t \simeq -0.5$ in helicity flip amplitudes for vector exchanges, there is now evidence for dips at $t \simeq -1.3$ in A_2 and f_o helicity flip amplitudes. The A_2 exchange dips are observed in $\pi^- p \to \eta^o n$ and $\pi^+ p \to \eta^o \Delta^{++}$ data.[75,62,60] [Figure 29]. The observation of a dip in $\pi^- p \to A_2^- p$ at 6 GeV was reported at this conference.[76] The $I_t = 0$ exchange contribution dominates in $\pi N \to A_2 N$ at high t, which suggests that the observed dip is associated with f^o (or possibly Pomeron) exchange.

The wrong signature nonsense zeros of Regge pole amplitudes occur at $\alpha = 0$ for vector exchanges and $\alpha = -1$ for tensor exchanges. This interpretation of the observed dips requires linearly falling trajectories. However it still seems unlikely that the A_2 trajectory falls sufficiently rapidly to intersect $\alpha = -1$ at $t \simeq -1.3$. In Regge cut models the dips would be generated as a result of pole-cut interferences.

E. Commentary

Although a coherent understanding of two body reactions is not yet achieved, there has been progress on various fronts. The t-channel approach accounts for the existence of exchange peaks, the energy dependences of reaction differential cross sections at near forward or backward angles, and the success of SU(3) relations. The absorption approach strives to retain the verified features of t-channel exchanges while modifying the t-dependence to peripheral form through rescattering

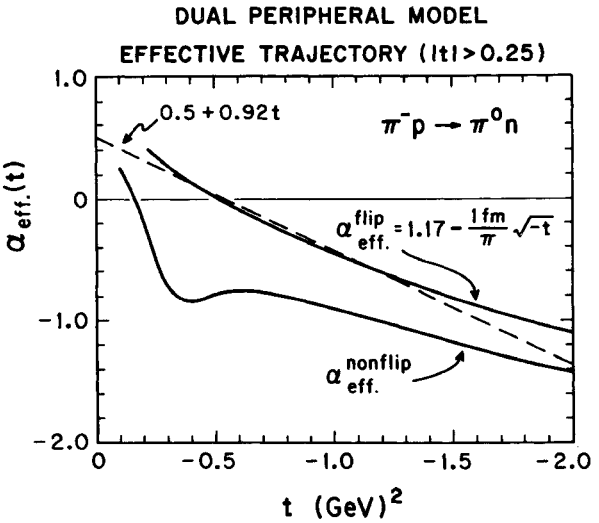

Figure 28: Effective t-channel Regge trajectory generated from s-channel Regge poles (from Ref. 71). The momentum ranges used were $6 \lesssim P_{LAB} \lesssim 48$ GeV for $\Delta\lambda = 1$ and $4 \lesssim P_{LAB} \lesssim 14$ GeV for $\Delta\lambda = 0$.

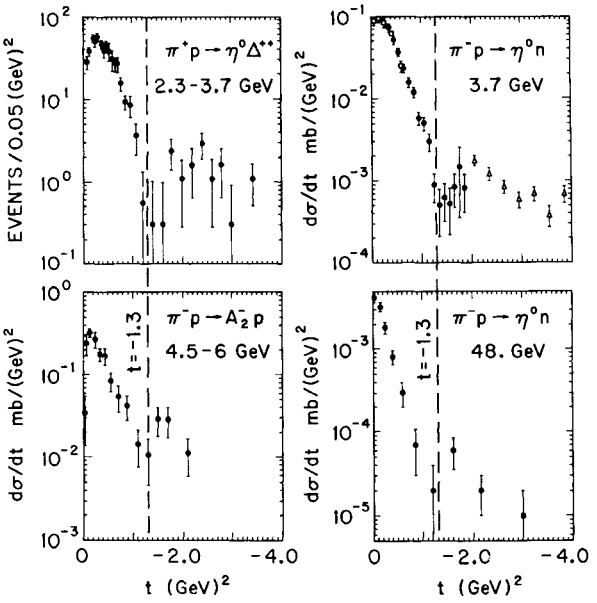

Figure 29: Observed dips at $t \simeq -1.3$ associated with A_2 and f_o exchanges. Data from Refs. 60, 62, 75.

[†] With a different parametrization of the s-dependence of the Regge residues, Chu and Hendry likewise find a more rapid s-dependence of the $\Delta\lambda = 0$ than the $\Delta\lambda = 1$ amplitude from a fit to $\pi^- p \to \pi^o n$ data [Ref. 72].

corrections. The s-channel approach uses duality with an effective s-channel peripheral trajectory to generate the t-dependence of amplitudes. It seems certain that an eventual comprehensive understanding will involve some sort of a merger of t-channel and s-channel viewpoints. Continued detailed study of the successes and shortcomings of the various approaches are needed to point the way to unification. The major challenge at present is to account for the observed qualitative differences between vector and tensor exchanges in both s and t dependence.

VIII DOUBLE CHARGE EXCHANGE REACTIONS: REGGE-REGGE CUTS

The double charge exchange reactions $\pi^- p \to K^+\Sigma^-$, $K^- p \to \pi^+\Sigma^-$, and $K^- p \to K^+\Xi^-$ afford an opportunity to search for Regge-Regge cuts since there are no known exotic meson candidates for single particle exchange. The expected high energy behaviour associated with Regge-Regge cuts at small t is[77]

$$\frac{d\sigma}{dt} \sim s^{2\alpha_{RR}-2} (\ell n\, s)^{-2}$$

where

$$\alpha_{RR}(0) = \alpha_1(0) + \alpha_2(0) - 1$$

For the $\rho + K^*$ cut, $\alpha_{\rho K^*}(0) \tilde{\sim} 0$ and the prediction is

$$\frac{d\sigma}{dt}(\pi^- p \to K^+\Sigma^-) \sim s^{-2}(\ell n\, s)^{-2}$$

The data on these double charge exchange reactions from 1.5 to 3 GeV exhibit an s^{-10} dependence characteristic of other exotic exchange channels such as $K^- p \to pK^-$, and $\bar{p}p \to p\bar{p}$ scattering at 180°. This precipitous behaviour at low energies is commonly ascribed to direct channel resonances. Recent Michigan measurements[78] above 4 GeV show a flattening trend in the energy dependence of the $\pi^- p \to K^+\Sigma^-$ section, consistent with a crude $\rho + K^*$ cut expectation that

$$s^2 \frac{d\sigma}{dt}(\pi^- p \to K^+\Sigma^-) \sim \text{constant}$$

[Figure 30]. The differential cross sections for $\pi^- p \to K^+\Sigma^-$ and $K^- p \to \pi^+\Sigma^-$ are approximately equal around 5 GeV, as would be expected for a $\rho + K^*$ cut mechanism.

Since the ρ (and A_2) Regge exchange amplitudes are dominantly helicity flip and the K^* amplitudes are dominantly helicity non-flip, the $\rho + K^*$ cut contribution should be flip dominated. The $\pi^- p \to K^+\Sigma^-$ data show a sharp decrease near $t' = 0$ characteristic of helicity flip contributions.

Calculations of the magnitude of double exchange contributions depend on assumptions about the intermediate states which are included,[79] but rough estimates are within the ball park of these experimental results for meson-meson cuts.

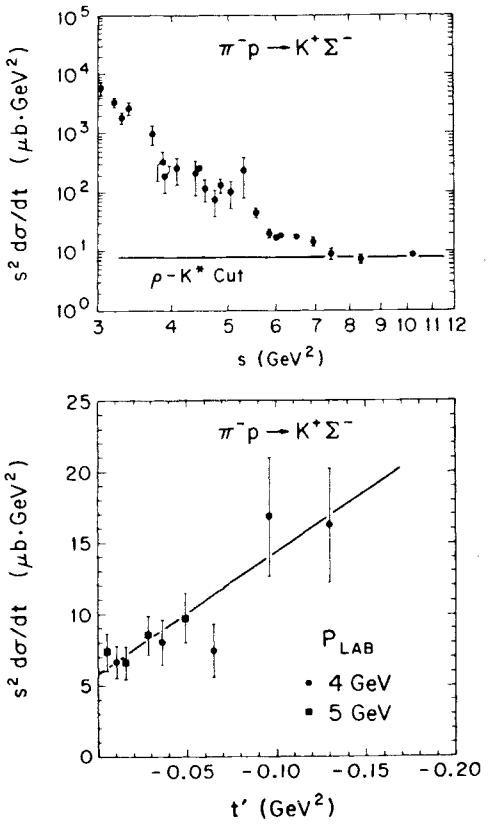

Figure 30: Comparison of recent $\pi^- p \to K^+\Sigma^-$ data (Ref. 78) with ρ-K^* cut expectations of a) $s^2 \frac{d\sigma}{dt} \sim$ constant and b) a sharp turnover near the forward direction.

Experimental studies of $K^-p \to pK^-$ backward scattering have not produced any evidence for meson-meson cuts. The 180^0 scattering data continue to show an s^{-10} decrease up to 6 GeV.[80]

IX THE CROSSOVER PHENOMENA

Elastic differential cross section differences

$$\Delta\left(\frac{d\sigma}{dt}\right) = \frac{d\sigma}{dt}(A^-N) - \frac{d\sigma}{dt}(A^+N)$$

cross from positive to negative values at a momentum transfer $t_c \sim -0.1$ to -0.2. To a good approximation this difference is proportional to the imaginary part of the helicity non-flip vector exchange amplitude

$$\Delta\left(\frac{d\sigma}{dt}\right) \propto \text{Im } V_{\Delta\lambda=0}$$

There is considerable interest in the question of how the crossover location changes with energy. In the unlikely case of a single factorizable Regge pole t_c would be energy independent. For a geometrical model,

$$\text{Im } V_{\Delta\lambda=0} \propto J_0(R\sqrt{-t}),$$

the crossover moves towards smaller $|t|$ if the radius increases with energy. For a pole-cut interference interpretation of the crossover

$$\text{Im } V_{\Delta\lambda=0} \propto \left[1 - c(t)\,\frac{s^{(\alpha_R' - \alpha_c')|t|}}{\ln s}\right]$$

the crossover moves inward in $|t|$ as the cut contribution increases relative to the pole for $t \neq 0$ (since $\alpha_R' > \alpha_c'$). However in current absorption models which have $\alpha_c' \approx \alpha_R'$ below 20 GeV, the crossover moves dramatically outward in $|t|$ at intermediate energies.[40,66,81]

Unfortunately few high precision experimental determinations of the crossover location have been made. Present direct experimental determinations are limited to $\pi^{\pm}p$, $K^{\pm}p$, $p^{\pm}p$ crossovers from Argonne at 3, 4, 5 and 6 GeV.[82]

Further information about crossovers can be deduced from experiments not specifically designed to measure this quantity which provide accurate particle and antiparticle slope determinations but have overall normalization uncertainties. At small t the exponential parametrization of the differential cross section is

$$\frac{d\sigma}{dt} = \frac{\sigma_t^2}{16\pi}\left[1 + \rho^2\right] e^{Bt}$$

where ρ = Re F/Im F at $t = 0$. Since at t_c,

$$\frac{d\sigma}{dt}(\bar{p}p) = \frac{d\sigma}{dt}(pp),$$

the cross-over location is given by

$$-t_c = \frac{\ln\left[\dfrac{\sigma_t^2(\bar{p}p)}{\sigma_t^2(pp)}\;\dfrac{1+\rho^2(\bar{p}p)}{1+\rho^2(pp)}\right]}{\left[B(\bar{p}p) - B(pp)\right]}$$

Accurate data for the σ_t's exist at most energies and the ρ's can be determined from dispersion relations. Hence data on the elastic slopes at $t = 0$ will suffice to determine t_c. Determinations of t_c in this manner from Serpukhov data[9,64] and preliminary SLAC[83] and NAL data[20] are shown in Figure 31.

X. SCATTERING AT LARGE ANGLES: PARTON MODELS

The recognition that large angle hadron scattering might be explained in terms of the scattering of point-like constituents ranks among the most exciting of recent developments in studies of exclusive reactions. A qualitative suggestion of a constituent mechanism from two body reaction data at large angles is the occurrence of fixed angle features and absence of prominent fixed t or fixed u structures associated with hadron exchange mechanisms. A series of theoretical and phenomenological investigations of constituent models for hadron scattering[84,85] led to the following simple quark model rule which correlates with the number of constituents of the external hadrons both

(i) the behaviour of the electromagnetic form factors at high momentum transfer

$$F_i(t) \sim t^{-n_i+1} \qquad \text{(large t)}$$

(ii) the energy dependences of two body cross sections at high s and fixed cm angle θ.

$$\frac{d\sigma}{dt} \sim s^{2-\Sigma n_i} f(\theta) , \qquad \text{(large } s,\theta)$$

This rule was proposed by Matveev-Muradyan-Tavkhelidze[86] and Brodsky-Farrar[87]. Here n denotes the number of constituents in the hadron (n_{meson} = 2, n_{baryon} = 3, n_{photon} =1, n_{lepton} =1) and the summation is over the external hadrons in the reaction.

This rule reproduces the experimentally observed monopole pion and dipole nucleon form factor behaviours (Figure 32). On the following reactions for which there exists a substantial amount of data the formular gives the fixed angle energy dependences:

reaction	fixed angle cross-section
$pp \to pp$, $\bar{p}\bar{p} \to \bar{p}\bar{p}$, $pp \to pN^*$	$d\sigma/dt \sim s^{-10}$
$\pi p \to \pi p$, $Kp \to Kp$	$d\sigma/dt \sim s^{-8}$
$\gamma p \to \pi N$, $\gamma p \to \pi \Delta$	$d\sigma/dt \sim s^{-7}$

Comparisons with experiment in Figure 33 indicate remarkable agreement.† Similar results have been found for the reactions $\bar{K}^o p \to \pi^+(\Lambda,\Sigma^o)$ and $K_L^o p \to K_S^o p$.[89] Attempts to simultaneously account for energy and angular dependences by constituent models have not been as successful, but such efforts are continuing.[90] The above energy dependences also follow from a generalized Wu-Yang expression

$$\frac{d\sigma}{dt}(AB \to CD) \sim \frac{1}{s^2} |F_A(t)F_B(t)F_C(t)F_D(t)|^2$$

when an electromagnetic form factor dependence t^{-n_i+1} is specified.[84] The results may also be derivable from an absorbed Regge exchange model with form factor residues.[81]

† The data in Fig. 33 have momentum transfers greater than 2.5 GeV^2 for pp→pp and πp→πp reactions and greater than 1 GeV^2 for the other reactions.

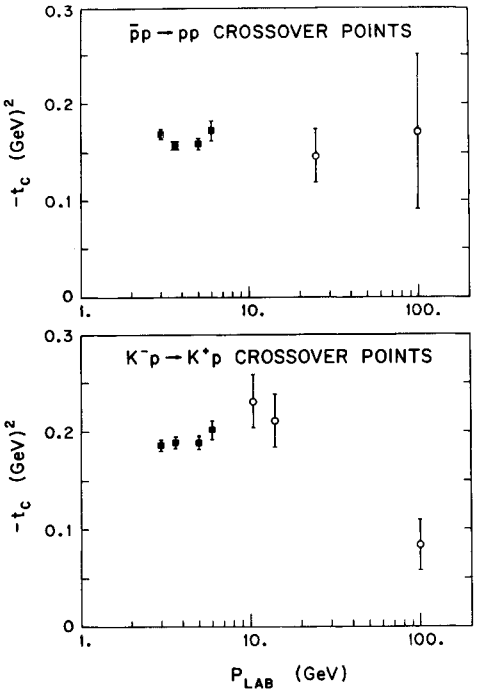

Figure 31: Cross-over locations of particle-antiparticle forward elastic peaks.

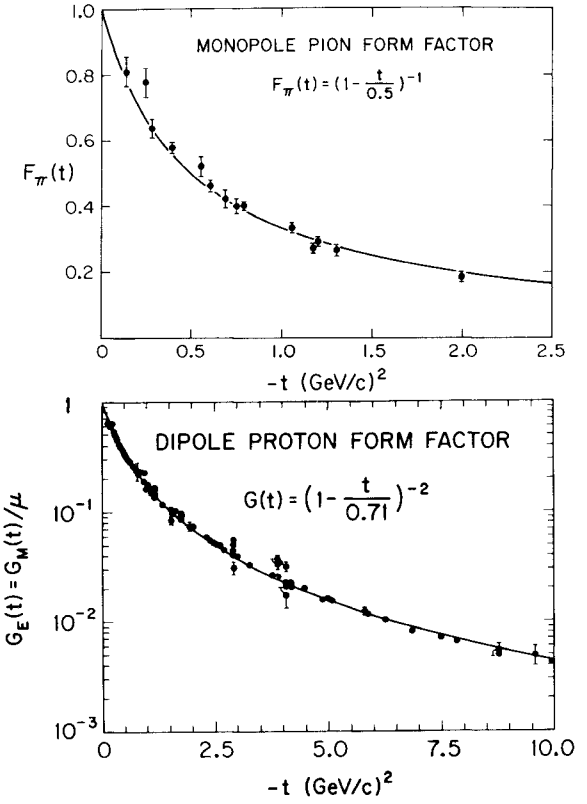

Figure 32: Electromagnetic form factors of pion (monopole) and proton (dipole).

The theoretical foundation of the quark constituent rule for the energy dependences of large angle scattering remains uncertain. The result can be obtained from a class of field theory diagrams based on the exchange of a neutral vector gluon, with assumptions about hadron-quark wave functions and quark-quark scattering.[87] However it has been pointed out that other diagrams which violate the conjecture should actually dominate at high s.[91] The leading diagrams in massive Q.E.D. also yield a behaviour different from the quark counting result.[92]

As a parting comment, Figure 34 illustrates the real art of phenomenology. Theoretical interpretations at times depend on how the data are plotted. Unfortunately more than one interpretation is sometimes possible as is the case here.

Acknowledgements

I wish to than J Luthe, W Long, K Geer, G Weller, T Weiler, J Kapusta and R Dudley for their dedicated efforts in preparation of materials for this talk. I am very grateful to R J N Phillips and F Halzen, for very helpful advice and many comments on the contents. I also thank G Kane, R Field and P Fischbane for useful discussions. The valuable assistance of scientific secretaries K Barnham and K Paler and session organiser R Field is greatly appreciated. Finally, I wish to thank W Baker, D Meyer and R Prepost for advance communication of data.

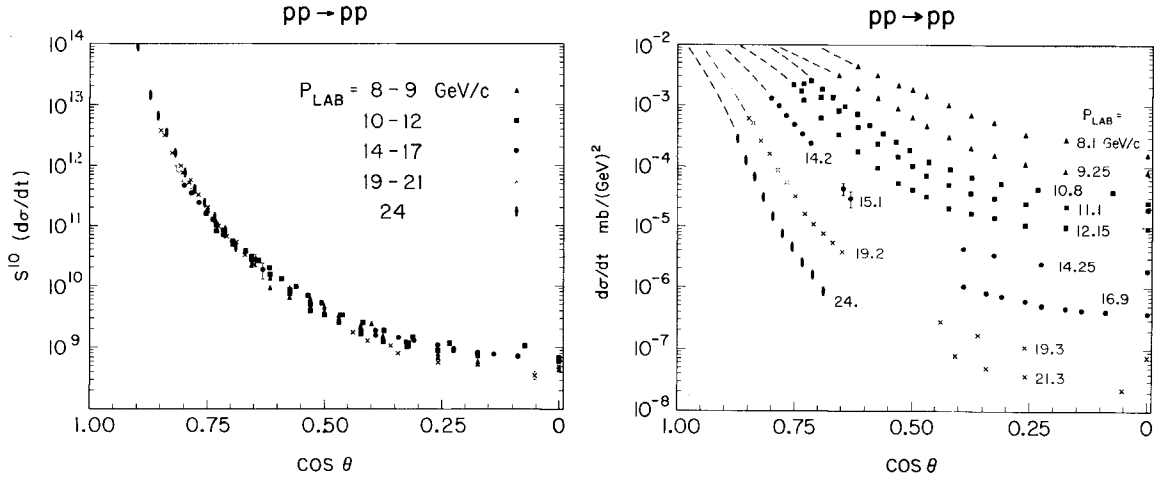

Figure 33: Experimental comparisons with the quark model rule

$$s^{\Sigma n_i - 2} \frac{d\sigma}{dt} = f(\theta)$$

for large angle hadron scattering

33a) $pp \to pp$ (s^{10})

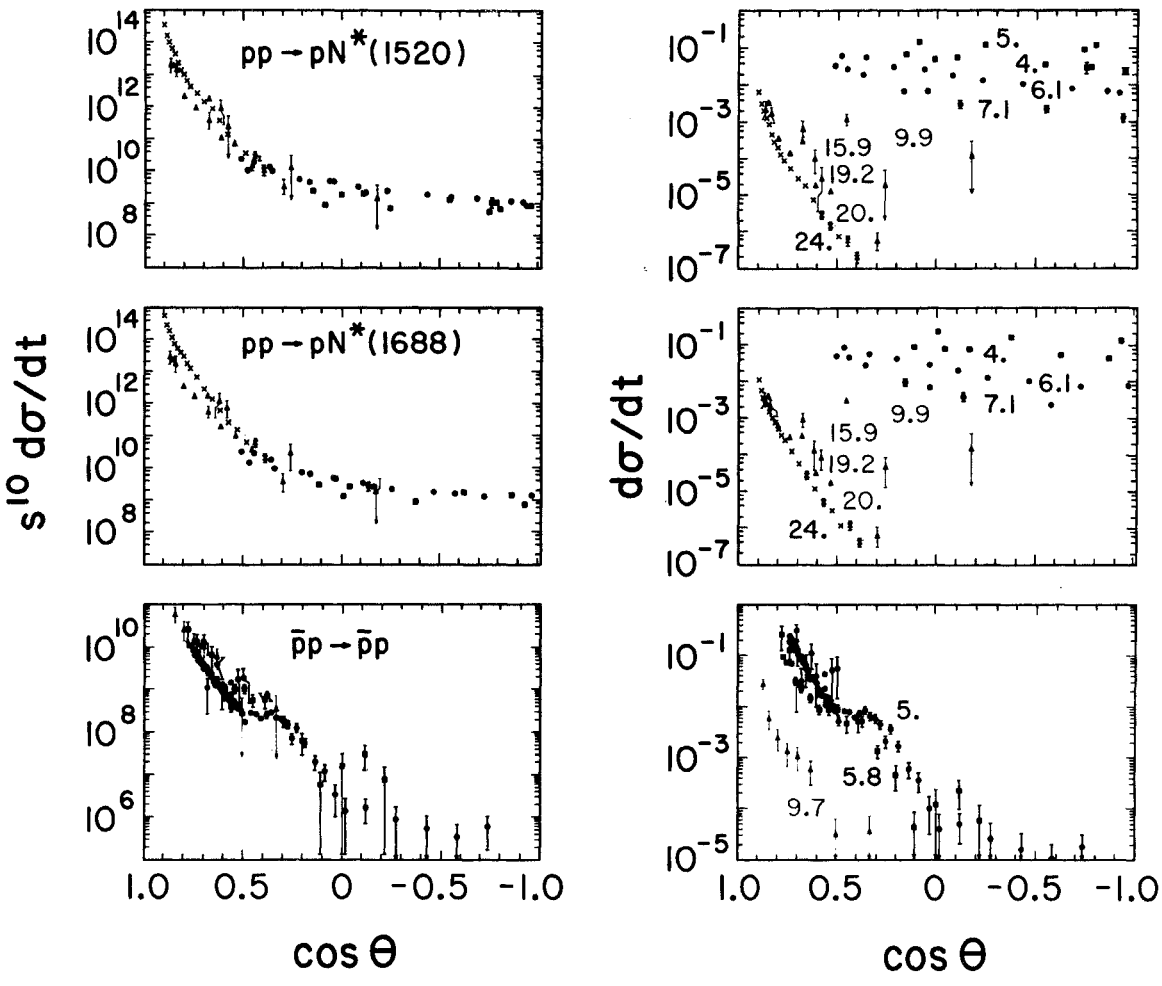

33b) $pp \to pN^*$, $\bar{p}p \to \bar{p}p$ (s^{10})

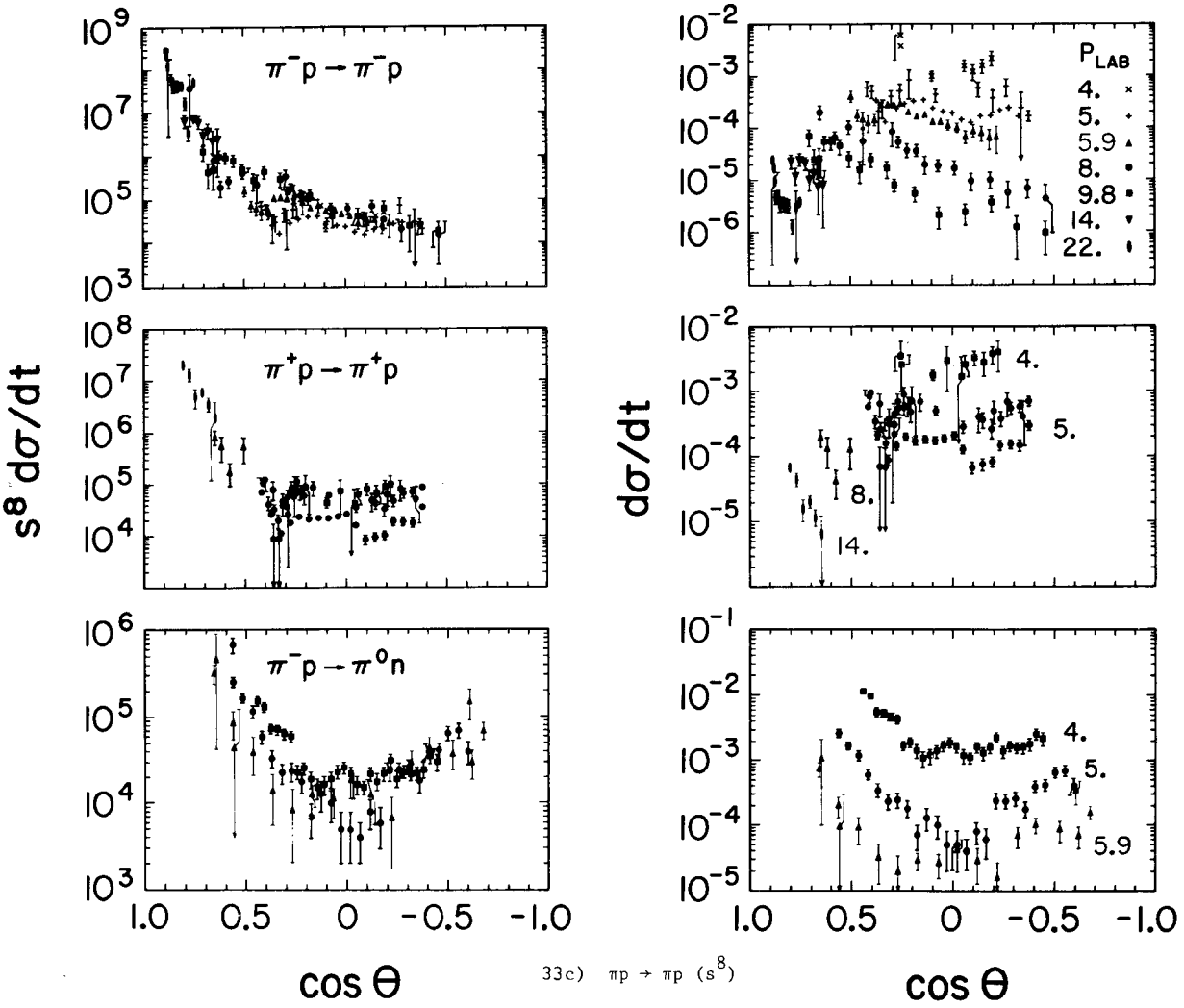

33c) $\pi p \to \pi p$ (s^8)

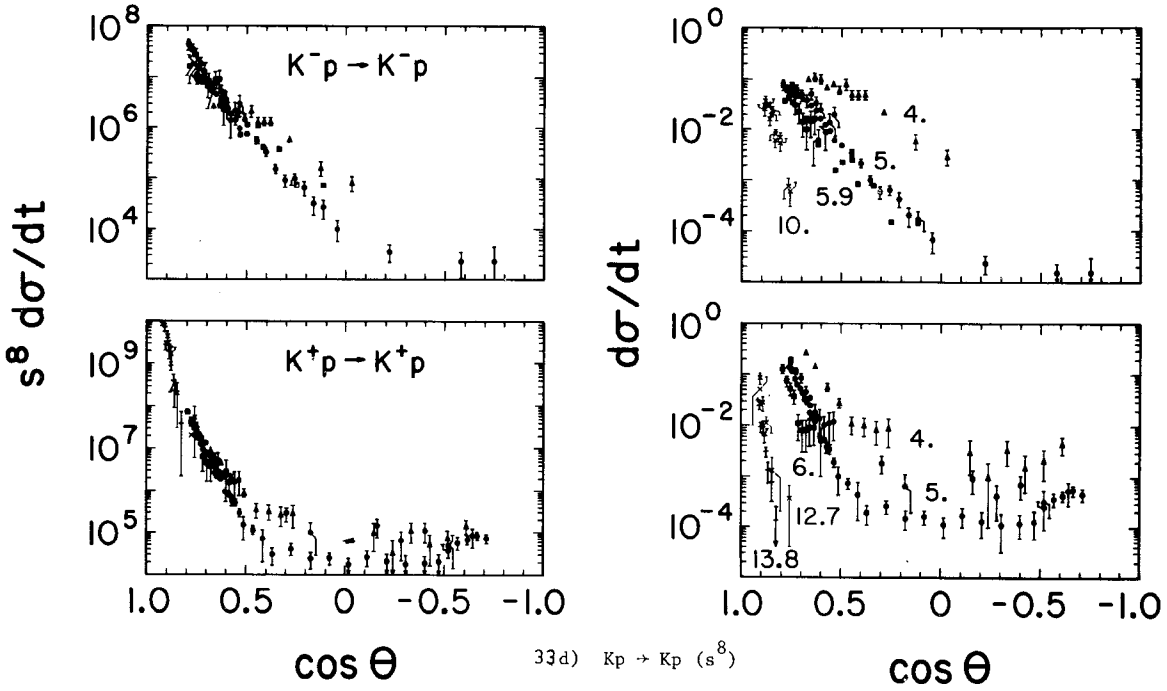

33d) $Kp \to Kp$ (s^8)

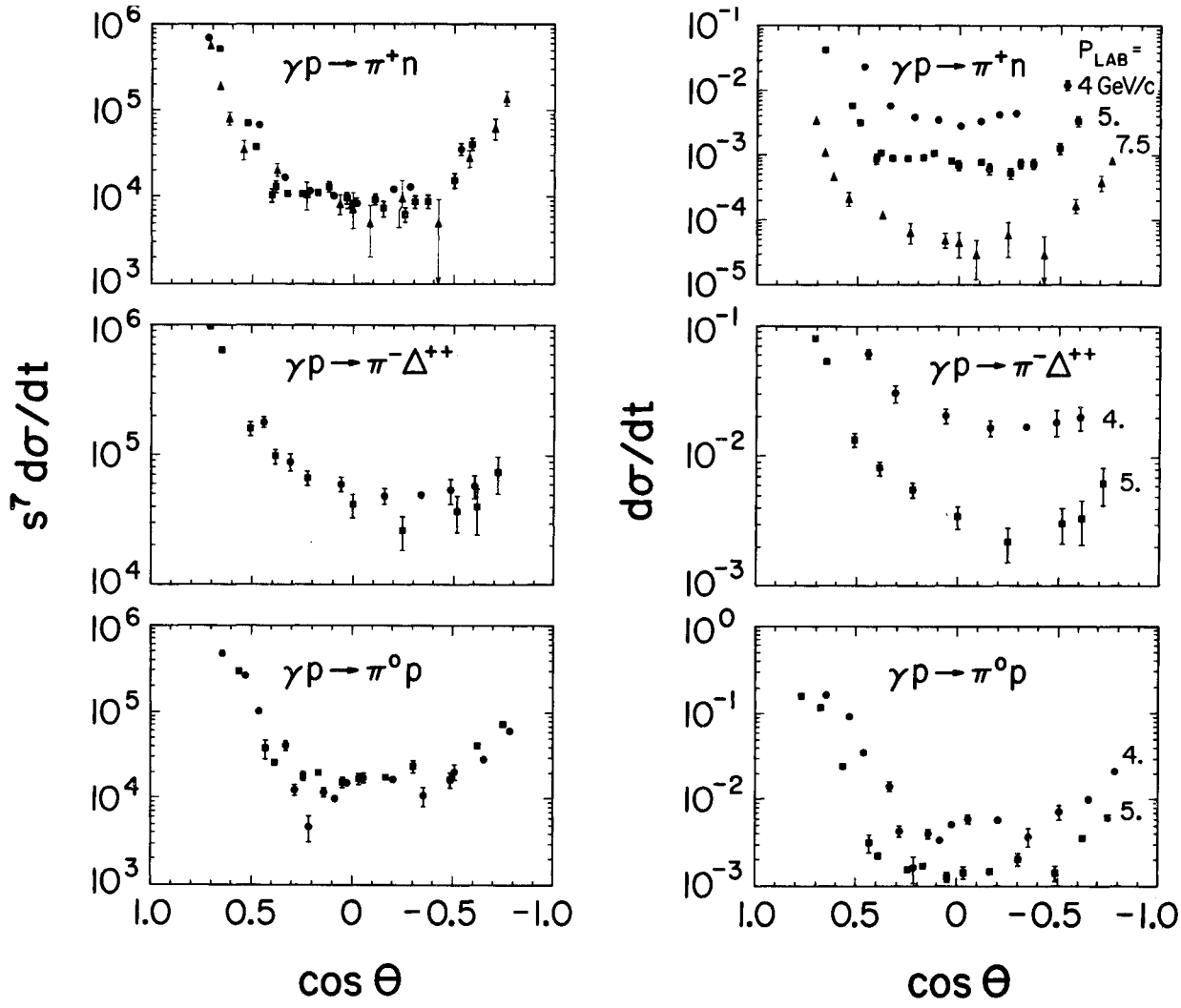

33e) $\gamma p \to \pi N, \gamma p \to \pi \Delta$ (s^7): unpublished data from Ref. 88.

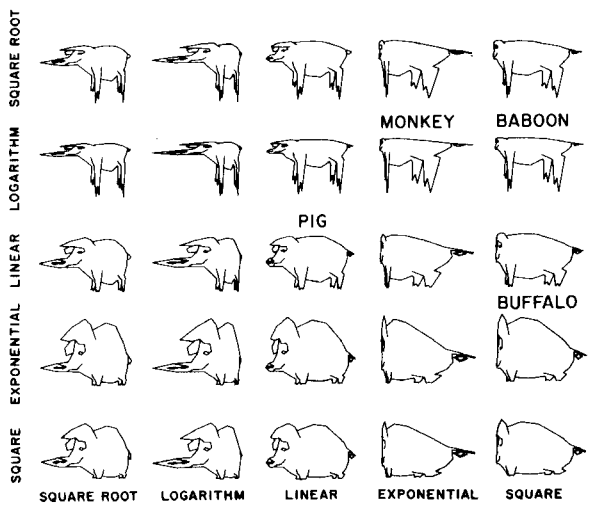

Figure 34: The art of phenomenology.

References

1. U Amaldi, et al., Phys,Letts. 44B, 112 (1973); S T Amendolia, et al., Phys.Letts. 44B, 119 (1973).
2. R Blankenbecler, J R Fulco, R L Sugar, SLAC-PUB-1281, (1973).
3. S J Chang, T M Yan, SLAC-PUB-1381 (1974).
4. P M Fishbane, J G Schaffner, J S Trefil, University of Virginia preprint (1974).
5. P Camillo, P M Fishbane, J S Trefil, University of Virginia preprint (1974).
6. G Barbiellini et al., Phys.Letts. 39B, 663 (1972).
7. U Amaldi et al., Phys.Letts. 36B, 504 (1971).
8. V Bartenev et al., Phys.Rev.Letts. 29, 1755 (1972).
9. G G Beznogikh, et al., Nucl.Phys. B54, 78 (1973).
10. F Halzen in Praticle Interactions at Very High Energies (Plenum Press, New York) (1974).
11. J D Jackson, LBL Report 2079 (1973).
12. J B Bronzan in Symposium on the Pomeron, ANL HEP-Report 7327 (1973).
13. J B Bronzan, G L Kane and U P Sukhatme, NAL-PUB-74-23-THY, (1974).
14. G Hohler, Karlsruhe preprints TKP 17/73, 4/74.
15. V Barger, K Geer and R J N Phillips, Nucl.Phys. B47, 29 (1972).
16. R C Fernow, S W Gray, A D Krisch, H E Miettinen, J B Roberts, K M Terivilliger, W de Boen, E F Parker, L J Ratner, J R O'Fallon, Conference paper 899 and 1010;
    F Halzen, Conference paper 965
    F Halzen, G H Thomas, Conference paper 966.
17. A Bohm, M Bozzo, R Ellis, H Foeth, M I Ferrero, G Maderini, B Naroska, C Rubbia, G Sette, A Stande, P Strilin, G de Zorzi, CERN Report (1974);
    E Nagy, M Regler, W Schmidt-Parzefall, K Winter, A Brandt, G Flügge, F Niebergall, K R Schubert, P E Schumacher, G Broll, G Coignet, J Favier, L Massonet, M Vivaagent, W Bartle, H Dibou, Ch. Gottfried, G Neuhofer, Conference paper.
18. A J Buras, J Dias de Deus, Nucl.Phys. 71B, 481 (1974).
19. R J N Phillips, Rutherford Laboratory, Report 034 T.80 (1974).
20. C W Akerlof, R Kotthaus, J A Koschik, R L Loveless, D I Meyer, I Amats, W T Meyer, C E W Ward, D P Eartly, R A Lundy, S M Pruss, D D Yovanovitch, D R Rust, University of Michigan, Report 74-20.
21. L Van Hove, Nuovo Cimento 28, 798 (1963), Rev. Mod. Phys. 36, 655 (1964).
22. R Henzi, P Valin, Phys.Letts. 48B, 119 (1973).
23. H I Miettinen, CERN Report TH 1864 (1974).
    E H de Groot, H I Miettinen, in Proceedings of VIIIth Recontre de Moriond, Vol.II (1973).
24. F S Henyey, R Hong Tuan, G L Kane, University of Michigan preprint, UM HE 73-18.
25. U Amaldi, CERN Report NP 73-19 (1973).
26. T Inami, R J N Phillips, R G Roberts, Rutherford Report (1974).
27. L Caneschi, Phys.Rev.Letts 23, 254 (1969).
28. T T Chou, C N Yang, Phys.Rev. 170, 1591 (1968); Phys.Rev. 175- 1832 (1968).
29. L Durand, R Lipes. Phys.Rev.Letts 20, 637 (1968).
30. J N J White, Nucl.Phys. B51, 23 (1973); GIFT-Madrid Report 7-73.
31. M Kac, Nucl.Phys. B62, 402 (1973);
    N Byers, in Proceedings of XIth International School of Subnuclear Physics, Erice, Sicily (1973).
32. F Hayot, U P Sukhatme, University of Michigan preprint, UM HE 73-31.
33. R Henzi, B Margolis, P Valin, McGill University Report (1974).
34. H Cheng, J K Walker, T T Wu, Phys.Letts. 44B, 97 (1973);
    J K Walker, in Proceedings of the VIIIth Recontre de Moriond, Vol. II (1973);

T T Wu, H Cheng, in AIP Conference Proceedings No. 15 (1973);
H Cheng, J K Walker, T T Wu, Conference paper No. 744.

35. C B Chiu, R J Gleiser, K H Wang, University of Texas preprint CPT-34 (1973).
36. P D B Collins, F D Gault, A Martin, Phys.Letts. 47B, 171 (1973) and Univ. of Durham Report (1974); A Martin, Univ. of Durham Report (1974).
37. N S Craigie, G Preparata, University of Hamburg preprint (1974).
38. N W Dean, Iowa State University Report (1974).
39. G Kane, Phys.Letts. 40B, 363 (1972); ANL HEP-Report 7327 (1973).
40. B J Hartley, G L Kane, Nucl.Phys. B57, 157 (1973).
41. J W Alcock, N Cottingham, C Michael, Nucl.Phys. 67B, 445 (1973).
42. J Pumplin, F Henyey, G L Kane, University of Michigan preprint (1974).
43. G Cohen Tannoudji, F S Henyey, R Hong Tuan, Saclay preprint, Conference paper 498.
44. W F Baker, A S Carroll, I-H Chiang, R L Cool, D P Eartly, O Fackler, G Giacomelli, P F M Koehler, T F Kycia, K K Li, P O Mazua, P Mockett, K P Pretzl, D C Rahm, R Rubenstein, A A Wehmann, Conference paper 991.
45. S P Denisov, et al, Nucl.Phys. B65, 1 (1973).
46. W Galbraith, et al., Phys.Rev. 138B, 913 (1965).
47. A compilation of SU(3) and quark model relations can be found in V Barger and L Durand, Phys. Rev. 156, 1525 (1967).
48. H J Lipkin, Weizmann Institute preprint, (1974).
49. V Barger, D Cline, Phys.Rev. 156, 1522 (1967).
50. R Diebold, D S Ayres, A F Greene, S L Kramer, A J Pawlicki, A B Wicklund, ANL/HEP Report 7404 (1974).
51. S Banerjee, J R Campbell, G Hall, G May, D Miller, R S Orr, J E Allen, V A Bull, P V March, K O'Brian, Conference paper 453.
52. C B Chiu in Proceedings of the Workshop on Particle Physics at Intermediate Energies, LBL (1971).
53. G Girardi, C Godrecke, H Navelet, Saclay Report T/74-10 (1974).
54. C Ciapetti, et al., Nucl.Phys. B66, 350 (1973); F Halzen, et al, Nucl. Phys. B54, 199 (1973).
55. A B Wicklund, D S Ayres, R Diebold, A F Greene, S L Kramer, A J Pawlicki, ANL Report, Conference paper 100.
56. A Białas, K Zalewski, Nucl. Phys. B6, 449 (1968); ibid B6, 465 (1968); ibid B6, 478 (1968).
57. R D Field in AIP Conference Proceedings No. 13 (1973); R D Field et al., Phys.Rev. D6, 1863 (1972).
58. A D Martin, C Michael, R J N Phillips, Nucl. Phys. 43B, 13 (1972); C Michael in Proceedings of the XVI International Conference on High Energy Physics at Batavia (1972).
59. R Field, private communication; R Field, A B Wicklund, to be published.
60. W D Apel, H Müller, D Schingel, H Schneider, G Sigurdsson, H M Staudenmaier, A Thys, E Bertolucci, R Franceschini, M Givoletti, I Mannelli, G Pieriazzini, A Seribano, F Sergiampietri, M L Vincelli, Yu B Bushnin, S V Donskov, M I Grachev, A V Injakin, V A Kachanov, R N Krasnokutsky, A A Lednev, Yu V Mikhailov, Yu D Prokoshkin, R S Shuvalov, P Johnson, W Kittenberger, G Leder, R Oberparlaiter, M Pernika, M Steuer, Karlsruhe-Pisa-Serpukhov-LBL-Vienna Collaboration, Conference Report 536; V N Bolotov, V V Isakov, D B Kakauridze, V A Kachanov, V M Kutjin, Yu D Prokoshkin, E A Rasuvaev, V K Semenov, V A Senko, V G Bybakov, IHEP Reports 73-52, 73-57.

61.A Barnes, J Mellema, A Tollestrup, R Walker, O Dahl, R Johnson, R Kenney, M Pripstein, Cal-Tech-LBL, Conference Papers 1045 and 1046.

62.A V Stirling, et al., Phys.Rev.Letts. 14, 763 (1965);
P Sonderegger, et al, Phys.Letts 20, 75 (1966);
O Guisan, et al., Phys.Letts. 18, 200 (1965) and private communication.

63.G A Ringland, Suppl. Journal de Physique, 34, C1-292, (1973).

64.Yu M Antipov, et al., Nucl. Phys. B57, 333 (1973);
A A Derevchekov, et al., Phys.Letts. 44B, 367 (1974);
IHEP Report 73-76.

65.V Barger, R J N Phillips, Phys.Rev. 187, 2210 (1969).

66.B J Hartley, University of Copenhagen preprint (1974).

67.N F Bali, J W Dash, Argonne National Laboratory preprint, ANL/HEP 7370 (1974);
ANL/HEP 7372 (1973).

68. R D Field, D P Sidhu, BNL Report 18181 (1973).

69. H Harari, Ann. Phys. 63, 432 (1971);
Phys.Rev. Letts. 26, 1400 (1971).

70. E N Argyres, A P Contogouris, J P Holden, State University of Plattsburgh, N Y preprint (1974);
F Elvekjaer, B R Martin, CERN preprint TH 1806 (1974);
I S Barker, A Donnachie, J K Storrow, Daresbury Laboratory preprint DL3P 196 (1974);
J S Loos , J A J Matthews, Phys.Rev. D6, 2463 (1972);
J Barger, F Halzen, K Geer, Nucl.Phys. B49, 302 (1972).

71. B Schrempp, F Schrempp, Nucl.Phys. 54B, 525 (1973);
ibid. 60B, 110 (1973);
Proceedings of the 1Xth Recontre de Moriond (1974); CERN Report TH 1736 (1973); CERN Report TH 1812 (1974).

72. S Y Chu, A W Hendry, Indiana University preprint, 2009-57 (1974);
Phys.Rev. D4, 2743 (1971, ibid. 3282 (1971);
Phys. Rev. Letts. 25, 313 (1970).

73. Y Hara, T Kuroda, Y Takaiwa, Prog. of Theor. Phys. 51, 840 (1974);
Y Hara, T Kuroda, Conference paper 131;
M Imachi, T Oroguchi, S Otsuki, F Toyoda, Prog. Theo. Phys. 45. 1849 (1971), ibid. 47, 1958 (1972), ibid. 48, 210 (1972);
K Inoue, T Kawabe, M Uehara, Kyushu University preprint, Conference paper 66;
K Ghoroku, M Imachi, S Otsuki, F Toyoda, Kyushu University preprint, Conference paper 110.

74. Høgaasen, ACTA Norvegia Physica (1972);
J P de Brion, R Peschanshi, Conference paper 976.

75. E H Harvey, et al., Phys. Rev. Lett. 27, 885 (1971); W S Brockett, private communication;
D F Grether, G Gidal, Phys. Rev. Lett. 26, 792 (1971).

76. H A Gordon, M Habibi, I Stumer, K W Lai, Cal Tech Report 68-447 (1974).

77. R J N Phillips., Phys. Lett. 24B, 342 (1967);
N W Dean., Nucl. Phys. B7, 311 (1968);
C Michael, Phys. Lett. 29B, 230 (1969);
C Quigg., Nucl. Phys. B34, 77 (1971).

78. C W Akerlof, T K Caldwell, J Koschik, R Kotthaus, D I Meyer, B Springett, University of Michigan Report AT-74-4.

79. D W Duke, N W Dean, Iowa State University preprint (1974).

80. C Baglin, et al., Conference paper 404.

81. G Kane, University of Michigan preprint (1974).

82. I Ambats, et al., Phys. Rev. D9, 1179 (1974).

83. D Leith, SLAC Report 1130 (1973).

84. W R Theis., Phys. Letts. 42B, 246 (1972).

85. R Blankenbecler, S J Brodsky, J F Gunion., Phys. Letts. 39B, 649 (1972); SLAC-PUB-1183 (1973); D Horn, M Moshe., Nucl. Phys. B48, 557 (1972); CALT-68-382 (1973); P V Landshoff, J C Polkinghorne., Phys. Letts. 44B, 293 (1973); V Barger, F Halzen, R J N Phillips., Nucl. Phys. B61, 522 (1973).

86. V A Matveev, R M Muradyan, A N Tavkhelidze, Nuovo Cim. Lett. 5, 907 (1972).

87. S J Brodsky, G R Farrar., Phys. Rev. Lett. 31, 1153 (1973).

88. R L Anderson, D B Gustavson, H J Halpern, R Prepost, D M Ritson, D H Tompkins, G A Ubitsch, D Wiser, Conference paper 1089; R L Anderson, et al., Phys. Rev. Lett. 30, 627 (1973); R Prepost (private communication).

89. G W Brandenburg, et al., SLAC-PUB-1202 (1973).

90. P G O Freund, S Nandi, Conference paper 833; G Preparata., TH 1836 CERN Preprint (1974); K Kinoshita, Y Myozyo, Kyushu University Report HE-10 (1974); Y Igarashi, T Matsuoka, S Sawada, Nagoya University preprint, Conference paper 72.

91. J C Polkinghorne., Phys. Letts. 49B, 277 (1974); Z F Ezawa, University of Cambridge preprint, DAMTP 74/5 (1974).

92. I G Halliday, J Huskins, C T Sachrajda., Phys. Letts. 47B, 509 (1973).